# Ground Validation for the Tropical Rainfall Measuring Mission (TRMM)

David B. Wolff[1,2], D. A. Marks[1,3], E. Amitai[1,3], D. S. Silberstein[1,3], B. L. Fisher[1,2],

A. Tokay[1,4], J. Wang[1,2], and J. L. Pippitt[1,3]

[1]*NASA Goddard Space Flight Center, Laboratory for Atmospheres*

[2] *Science Systems & Applications, Inc.*

[3]*George Mason University, Center for Earth Observing and Space Research*

[4] *University of Maryland Baltimore County, Joint Center for Earth Systems Technology*

---

*Corresponding Author's Address:*
David B. Wolff
NASA/GSFC, Code 912.1, Greenbelt, MD 20771
wolff@radar.gsfc.nasa.gov

**Abstract**

An overview of the Tropical Rainfall Measuring Mission (TRMM) Ground Validation (GV) Program is presented. The validation program is based at NASA Goddard Space Flight Center in Greenbelt, Maryland and is responsible for processing several TRMM science products for validating space-based rain estimates from the TRMM satellite. These products include gauge rain rates, and radar-estimated rain intensities, type, and accumulations, from four primary validation sites (Kwajalein Atoll, Republic of the Marshall Islands; Melbourne, FL; Houston, TX; and Darwin, Australia). Validation site descriptions of rain gauge networks and operational weather radar configurations are presented together with the unique processing methodologies employed within the Ground Validation System (GVS) software packages. Rainfall intensity estimates are derived using the Window Probability Matching Method (WPMM), and then integrated over specified time scales. Error statistics from both dependent and independent validation techniques show good agreement between gauge-measured and radar estimated rainfall. A comparison of the NASA GV products and those developed independently by the University of Washington (UWASH) for a subset of data from the Kwajalein Atoll site also shows good agreement. A comparison of NASA GV rain intensities to satellite retrievals from the TRMM Microwave Imager (TMI), Precipitation Radar (PR) and Combined (COM) algorithms is presented, and it is shown that the GV and satellite estimates agree quite well over the open ocean.

## 1. Introduction

The Tropical Rainfall Measuring Mission (TRMM) is a satellite-based program to measure tropical rainfall and to help quantify the associated distribution and transport of latent heat, which drives the global atmospheric system. TRMM is a joint U. S. – Japan mission and was launched from Tanegashima, Japan, on November 27, 1997 (Simpson et al. 1996; Kummerow et al. 1998). TRMM has provided state-of-the-art precipitation measurements since shortly after launch and was boosted from its original 350 km orbit to a new orbit of 402.5 km in August 2001 in order to extend science observations beyond the original timeframe of 2000. A key effort of TRMM has been dedicated to providing ground validation (GV) of the satellite rainfall estimates. The GV program is based in the TRMM Satellite Validation Office (TSVO) at NASA Goddard Space Flight Center (GSFC) in Greenbelt, Maryland. The GV program has been collecting radar and rain gauge measurements since 1988 and continues to collect data sets at a number of sites located throughout the tropics.

The aim of this paper is to provide a summary of GV operations, algorithm descriptions, and data quality. A description of the primary GV sites and details of their operational configurations are provided in Section 2, including a description of the network of radar and rain gauge networks at each site. Section 3 discusses the software system and algorithms developed and maintained by TSVO for processing the data, details data sources and ingest methodologies, and provides a brief description of the Level I-III TRMM GV Science Products (TSP) and how they are produced. Section 4

provides a discussion on the error statistics of the radar rainfall estimates versus both dependent and independent gauge measurements, as well as a comparison of rain rates and monthly accumulations between TSVO and those produced by the University of Washington. Section 5 provides validation comparisons between TRMM GV and satellite-retrieved rain intensities generated by the TRMM Microwave Imager (TMI), Precipitation Radar (PR), and Combined (COM) algorithms.

## 2. Description of Current GV Operations

The original plan for the Global Validation Program selected 10 sites from various locations around the world for the purpose of climatological validation of the TRMM satellite precipitation estimates. Four of these sites were designated as Direct Data (DD) sites and six were designated as Direct Product (DP) sites. The four selected DD sites were Kwajalein, Republic of the Marshall Islands; Melbourne, Florida; Houston, Texas; and Darwin, Australia, and are the focus of this paper. The global distribution of these sites is provided in Fig. 1. Figure 2 provides a 5-year climatology of monthly rainfall totals derived from observed GV gauge data for the four DD sites. Figure 3 provides a 5-year climatology of the diurnal cycle of occurrence of precipitation for the four DD sites, generated from observed GV gauge data. Details on the site-specific properties of Fig. 2 and Fig. 3 will be provided in the following sections describing the individual sites.

*a. The GV Network at Kwajalein*

One of the primary goals of the TRMM Mission is to validate satellite rain estimates over the open ocean with independent estimates obtained from regional surface sensors. A GV site was established on Kwajalein (KWAJ) Atoll in the Republic of the Marshall Islands, in the central Pacific Ocean. KWAJ is located on the northern edge of the Pacific Inter-Tropical Convergence Zone (ITCZ) and on the eastern boundary of the western Pacific warm pool. The atoll consists of a ring of small, flat coral islets, which are part of the vast archipelago scattered across the central Pacific. These islets have no significant orographic features and are thickly overgrown with palm trees and other tropical vegetation.

Figure 2 provides the mean monthly and annual rainfall for KWAJ (and the other GV sites). The annual rainfall at KWAJ is dominated by convective systems that form in the ITCZ. Most of the rainfall occurs in association with the northward migration of the ITCZ between April and October, which leads to a strong south-to-north gradient of annual rainfall. During the northern hemispheric winter, the ITCZ migrates further to the south, producing a sharp (climatologically significant) increase in the trade winds. This increase is correlated with a decrease in total rainfall amounts and event frequency. Schumacher and Houze (2000) show that Kwajalein precipitation is also contributed to by a significant number of isolated, shallow (< 5 km) "warm rain" clouds.

Figure 3 shows the probability of occurrence of precipitation at each hour of the day (local time), and for KWAJ reveals a slight diurnal maximum between 0400-0600

LT, however, the amplitude is fairly weak and convective showers can occur at any time of the day with about equal probability (Wolff et al. 1995). The diurnal cycle for KWAJ shown in Fig. 3 is consistent with other studies of diurnal rainfall over the open oceans, with the existence of a low amplitude nocturnal maximum in rainfall, associated with enhanced instability due to radiational cooling at the tops of clouds (Kraus, 1963; Gray and Jacobson, 1977; Hendon and Woodbury, 1993).

Kwajalein Island is the command center for the Reagan Missile Testing Range of the United States Army at Kwajalein Atoll (USAKA), and weather operations conducted there primarily support military operations. The KWAJ radar is located on Kwajalein Island at 8.718° N latitude and 167.733° W longitude, and is generally operated in a volume scan mode consistent with the scientific objectives of TRMM. The data is collected on Exabyte (8 mm) tapes and sent routinely to NASA/GSFC. Kwajalein reflectivity data have spatial resolution of 250 m for each 1º in azimuth. Table 1 provides the general characteristics of the KWAJ radar, also referred to as KPOL. Table 2 provides a description of the scanning strategy employed by KPOL.

TSVO operations at KWAJ are currently limited to small islets that extend from Kwajalein Island at the southern tip of the atoll, to Roi Namur at the northern end. A map of the KWAJ GV radar and gauge network is provided in Fig. 4. The network of seven rain gauge sites (see Table 3) was first deployed in 1988 in an early phase of the TRMM GV program. The locations of the KWA gauge network are labeled as squares on the map in Fig. 4. Current operations include two gauges at every site, but there are

no gauge data available south of Kwajalein Island, or north of Roi Namur, which is approximately 75 kilometers from the radar.

*b. Central Florida*

Central Florida (MELB) was selected as another DD site for TRMM GV operations. The principal radar is located on the eastern Atlantic seaboard in Melbourne, Florida. The area observed by the radar is approximately 50% ocean and 50% land. Florida is a sub-tropical location that receives about 70% of its annual rainfall between June and September, as inferred from Fig. 2. Most of this rainfall is due to sea breeze induced isolated convective systems, and large organized tropical storms. Florida's annual rainfall budget also receives a contribution from mid-latitude synoptic systems during northern hemispheric winter months when frontal boundaries occasionally affect Florida weather.

The diurnal cycle of rainfall at MELB is highly periodic, being dominated by the frequent occurrence of sea breeze induced convection in the mid-to-late afternoon. The diurnal profile for MELB shown in Fig. 3 reveals a maximum in rain occurrence in the afternoon. In the summer months especially, this distinct climatological feature is connected with a periodic sea breeze/land breeze oscillation, that is coupled to the diurnal heating cycle. According to Fig. 3 over 50% of the total rain occurs between 1200 and 1800 local time.

The MELB site is complemented by a Weather Service Radar – 1988 Doppler (WSR-88D), which is located at 28.113° N latitude and 80.654° W longitude. Figure 4 is a map of the MELB site that provides the location of the radar and the associated rain gauge networks. Crum et al. (1993) provide more information on the WSR-88D system and operations.

TSVO receives data from a broad distribution of gauges spread across the MELB GV site, as shown in Fig. 5. Although the gauge sampling is quite good overall, the gauge density is variable from sector to sector and no coverage exists in the far western sector of the state at a distance greater than 100 kilometers from the radar, or over the Atlantic Ocean. Four separate networks provide data for GV efforts: Kennedy Space Flight Center (KSC), St. Johns Water Management District (STJ), South Florida Water Management District (SFL) and an 18-gauge (over a 48 $km^2$ area) dense scale network at the Triple-N ranch (NNN). The KSC and NNN networks are owned and operated by NASA. The STJ and SFL networks are operated by their Florida Water Management Districts. The number of gauges in each of these networks is shown in Table 3. Data is processed by TSVO on a month-to-month basis and special arrangements have been made with the site managers of each network for timely, routine transfer of the data to NASA GSFC.

*c. Southeast Texas*

The southeast Texas GV network (HSTN) is shown in Fig. 6. This site provides observational coverage for the coastal regions of Texas and western Louisiana and a large inland region north and west of Houston and also extends southward approximately 100 km into the Gulf of Mexico. The mean precipitation for the Houston area averages about 1200 mm $yr^{-1}$. Figure 2 does not suggest a strong mean seasonal cycle of monthly rainfall, but some variability is observed, with a maximum monthly rainfall observed in June (~205 mm). Regionally, however, there is a strong geographical west-to-east gradient in annual average precipitation, ranging from 600 mm $yr^{-1}$ in the west to over 1500 mm $yr^{-1}$ in the east. The mean diurnal cycle in Fig. 3 shows a relatively weak afternoon maximum, with only slight variation in the probability of precipitation as a function of the time of day. Florida and Darwin, for instance, show stronger afternoon amplitude, suggestive of more active convective heating cycle.

The primary radar for the Houston site is the WSR-88D located in League City, TX, at 29.472° N latitude and 95.079° W longitude. This radar has characteristics similar to the WSR-88D radar at MELB (Crum et al. 1993). Figure 6 provides a regional map of the Houston area, showing the radar and gauge locations. The gauges are maintained and operated by the Harris County Emergency Operations Center. As indicated in Fig. 6, most of the gauges are distributed around Harris County, Texas and around an axis extending about 100 km northwest of the radar. Consequently, the spatial sampling inferred from the density distribution of gauges varies markedly, with only a few gauges located near the coast and south of the radar. It should also be noted in Table 3 that the bucket size is 1.0 mm, four times larger than the standard 0.254 mm of the other GV

networks, excluding Darwin, which is 0.2 mm. The bucket size is important in the determination of rain rates inferred from the discrete time series of tips. The larger bucket size effectively reduces the time resolution of the rain rates in each rain event, as fewer tips are collected over a characteristically longer period, limiting the ability to calculate light rain rates.

*d. Darwin, Australia*

Darwin, Australia (DARW) is located on the north central coast of Australia and borders the southern edge of the Indonesian maritime continent. The radar coverage also includes Melville and Bathurst Islands, which exert a strong effect on the regional rainfall climatology. The annual cycle at Darwin is distinctly bi-modal, characterized by wet and dry seasons (Figure 2). The "rainy" season extends from November to April and accounts for over 90% of the annual rainfall. Keenan et al. (1992) classify two primary rain regimes around DARW during the rainy season: monsoon and break periods. Monsoonal periods are associated with a westerly maritime flow regime that is characterized by weak convection, but widespread regional coverage. Monsoonal pulses typically last less than a month and occur about three times in a given rainy season. Break periods are identified with an easterly continental flow regime characterized by deep convection in association with large organized propagating squall lines and smaller isolated convective systems. Some of the deepest convection in the world occurs over Melville and Bathurst Islands, about 50 km off the northern coast. Thunderstorms are observed over these islands 65% of the days during the break periods (Keenan and Carbone, 1992). The diurnal cycle at

DARW is highly variable, and to a large extent, regime dependent. Figure 3 shows a large maximum in the occurrence of precipitation in the afternoon and early evening hours. Much of this precipitation is contributed to by the massive thunderstorms that develop via sea-breeze convergence over the islands, and sea-breeze and air-mass convection over the mainland as well as nocturnal squall lines and widespread monsoonal rainfall.

The Darwin radar is located at 12.248° S latitude and 130.925° E longitude, and is operated and maintained by the Australian Bureau of Meteorology Research Centre (BMRC). The radar is operated only during the Summer Hemisphere summer (November through March) each year and generally in a surveillance mode of 15-30 minute volume scans and periodic base scans (low level only). During Special Observing Periods (SOP), the radar is operated in an enhanced mode with 5-15 minute volume scans and 5-minute base scans. Data from the Darwin (C-POL) radar are recorded with a variable spatial resolution ranging from 250 m to 1 km for every 1º in azimuth (Keenan et al. 1998).

The DARW gauge network is shown in Fig. 7. This gauge network provides regional coverage over land, though the gauges on west Melville Island dominate sampling over the islands. There are also a few higher resolution networks located to the southeast of the radar (not shown) that provide additional information on the scale-related variability of precipitation near Darwin and can be used for validation the radar rainfall estimates.

## 3. Ground Validation Science Data Products

In order for the TSVO to produce the myriad of products specified by the TRMM Science Team, a rather extensive package of programs and libraries were developed. The principal libraries are the Radar Software Library (RSL) and the Ground Validation System (GVS). These packages are available under the GNU Public License and can be obtained from the TRMM Office web server. RSL supports a number of different ingest formats, including Universal Format (UF), SIGMET ®, and WSR-88D Archive II. RSL also supports output in UF and HDF formats. Further information on RSL can be found at: http://trmm-fc.gsfc.nasa.gov/trmm_gv/software/rsl/index.html.

Figure 8 depicts the basic Level I and Level II processing flow of TRMM GV radar data. Data from MELB and HSTN are now received in near real time over the Internet via an arrangement with the WSR-88D OSF, the National Climatic Data Center (NCDC), and the NWS. Radar data from the other primary sites are collected on 8-mm tapes and sent directly to GSFC. Data from Kwajalein usually arrive on a bi-weekly basis. Darwin data is received in 2 or 3 batches throughout the rainy season. Radar data are collected from the Houston, Melbourne, and Kwajalein sites on a year-round basis, while Darwin data are collected only during the rainy season (November through April).

. Radar data are processed into two standard TRMM GV Level I products using the GVS software package (Marks et al. 2000; Kulie et al. 1999). Two primary Level I

processing tasks are performed, converting radar data into a common format for archival, and quality control (QC) of the reflectivity data. Level I products are in polar coordinates and are written in Hierarchical Data Format (HDF) to conform to official archival standards of the DAAC. For brevity, Table 4 provides a description of the TSP for Levels I, II and III. Details on the more important aspects of their generation, specifically the means by which the radar rainfall estimates are produced, are discussed in the following section. Marks et al. (2000) provide more extensive detail on the available GV products.

## 4. Radar Rainfall Estimation

Many researchers have addressed the issue of rainfall estimation from radar. Summaries can be found, for example, in Wilson and Brandes (1979), Doviak (1983), Austin (1987), Atlas (1987), and more recently, Atlas et al. (1997). The approach adopted by the TRMM GV program at NASA GSFC is to use operational rain gauge networks and ground-based radar data to derive $Z_e$-R relationships and precipitation estimates. An integral part of this process is the evaluation of product quality or the degree of confidence we have in the accuracy of the estimates. Rain gauges serve a key function in capturing point measurements of surface rainfall. Networks of gauges with broad spatial distributions allow the best opportunity for meaningful comparison with ground-based radar.

Rain gauges are precision instruments that need to be adequately calibrated in the laboratory prior to deployment in the field and at regular intervals thereafter. Rain gauges are also subject to the elements and suffer complications due to typical weathering of the harsh tropical environments in which they are deployed. Data dropouts can and do occur related to short duration glitches or longer term failures of on-board loggers. A description of sampling errors of tipping bucket rain gauge measurements can be found in Habib et al. (2001) and Ciach et al. (1997). A persuasive argument can be made for a system of densely spaced gauges to provide sufficient spatial coverage as well as multiple gauges at each individual location to provide redundancy, and to mitigate the impact of mechanical breakdown on data collection efforts.

*a. Data Extraction and Merging for* $Z_e$-R *Development*

Official GV rainfall products are developed in modular steps with distinct intermediate products. These developmental steps include: (1) extracting quality-controlled radar data over the locations of rain gauges; (2) merging gauge and radar data in time and space; (3) automated QC of radar and gauge merged data; and (4) deriving $Z_e$-R lookup tables for converting observed radar reflectivities into rain intensities from the merged data.

In the first step, reflectivity data from the 2A-55 product is extracted over validation rain gauge locations. Data from the 1.5 km and 3.0 km Constant Altitude Plan Position Indicator (CAPPI) levels are extracted from each radar volume scan (over the

course of 1 month) from the pixel over rain gauge locations. Each radar pixel size is 2 km x 2 km and the extracted gauge data is from the 7 minutes centered at the radar volume scan time, as explained in more detail by Amitai (2000).

The rain gauge data are then merged in time and space with the extracted reflectivities to create a second intermediate (merged) file for $Z_e$-R development. Up to this point, independent QC techniques have been applied to both the radar and rain gauge data. An automated QC algorithm (Amitai, 2000) is applied to the combined radar and rain gauge data to determine which rain gauges (on a monthly scale) are unreliable for the purposes of $Z_e$-R development. The reliability of a particular rain gauge is determined upon comparison with the associated radar data above the gauge location. When a gauge is considered unreliable for a particular month, all data from both the gauge and extracted radar pixels above that gauge are filtered from the merged file. This procedure ensures that only objectively determined "good" gauges are used in the monthly WPMM $Z_e$-R development. WPMM matches the probabilities of radar observed reflectivities $Z_e$ and gauge measured rain intensity $R$ in such a way that the probability density function (PDF) of the radar estimated R above the gauge will be identical to the PDF of the gauge rates on a monthly scale. The resulting $Z_e$-R functions are found to be curved lines in log-log space rather than a straight-line power law (Rosenfeld et al. 1994).

Moreover, the PDF of the gauge rates was found to better represent the true PDF of R at the scale of a radar pixel than the one based on application of a gauge adjusted power Z-R relationship (Amitai et al. 2004). Therefore, the application of the WPMM $Z_e$-

R relationships will allow better evaluation of the instantaneous rainfall based on comparing the satellite–based PDF of R with PDF derived from coincident ground observations (Amitai et al. 2003).

*b. Site Specific Considerations and Challenges*

Due to the inherent characteristics of the available GV networks, owing mostly to geography and logistical realities, different techniques for deriving the $Z_e$-R relationships must be employed.

At MELB, monthly unconditional distributions of $Z_e$ and R from the QC merged data are used to derive specific month-to-month $Z_e$-R lookup tables. The Melbourne WSR-88D radar is stable and well calibrated, which allows the WPMM technique to be applied on a month-to-month basis (Anagnostou 2001). In order to mitigate range effects on the results (Rosenfeld et al. 1992), multiple-range (15-50 km, 50-98 km, and 98-150 km) $Z_e$-R relationships are used. There are three rain gauge networks with gauges distributed throughout all ranges (see Fig. 5). For a given month, each range has its own uniquely determined WPMM $Z_e$-R lookup table based on the unconditional distributions of $Z_e$ and R found within that range. $Z_e$ distributions are obtained by extracting reflectivity from specific CAPPI heights directly over gauge locations. For the closest ranges (15-50, and 50-98 km), NCAR Sorted Position Radar Interpolation (SPRINT) interpolated reflectivities are extracted from the 1.5 km CAPPI height over validation gauge locations. For the outer range (98-150 km), the interpolated reflectivities are

extracted from the 3.0 km CAPPI height over validation gauge locations. Resulting WPMM $Z_e$-R lookup tables are then applied directly to the same CAPPI levels from which they were derived to obtain instantaneous rain rate map products (TSP 2A-53). No distinction between convective and stratiform classifications in $Z_e$-R development.

Monthly rainfall accumulation products (TSP 3A-54) are obtained by integrating the instantaneous rain rate maps over time. Integration parameters are defined by the time difference $\Delta T$ between successive radar volume scans. This scheme assumes that instantaneous rain rates remain constant for the duration of the specific radar scan up to a maximum $\Delta T$ of 10 minutes. When $\Delta T$ exceeds 10 minutes, the rain rate map immediately following the data gap is integrated for 5 minutes. The 5-minute period was chosen as it represents the approximate time required to complete the WSR-88D volume scan. This integration scheme is applied to all radar volume scans for each month at the Melbourne, Florida validation site.

At KWAJ, the lack of “good” gauge data provides unique circumstances that require different techniques than those employed at MELB. For KWAJ, monthly WPMM $Z_e$-R development is not performed due to the limited number of rain gauge sites. On average, data from less than 7 "good" gauges are available each month. To circumvent this problem, and to create adequate $Z_e$ and R distributions, QC'd radar and gauge merged data from the entire year of 2002 were combined. This large-scale data compilation procedure captures a full spectrum of precipitation events, and provides robust distributions for WPMM $Z_e$-R development. Because most of the good gauges are

within 98 km of the Kwajalein S-band polarimetric radar, we take a special approach to the $Z_e$-R development. SPRINT-interpolated reflectivity data are extracted over the gauge locations from both the 1.5-km and 3.0-km CAPPI levels. Data from the 1.5-km (3.0-km) level are used in the $Z_e$ distribution to develop a $Z_e$-R lookup table for the 15-98 km (98-150 km) range. By this technique, we are assuming that the $Z_e$-R distributions obtained from radar and gauges within 98-km can be used to develop $Z_e$-R lookup tables which are applied to the areas both inside and outside 98 km. The monthly rainfall accumulation scheme employed at KWAJ is very similar to MELB in that the instantaneous rain rate maps are integrated over the time difference $\Delta T$ between successive radar volume scans. The maximum $\Delta T$ for integration is 15 minutes. If $\Delta T$ exceeds 15 minutes, the rain rates from the instantaneous map immediately following the gap are integrated for 10 minutes. The 10-minute period was chosen as it represents the approximate time between successive volume scans (with the current scanning strategy).

The calibration of the KWAJ radar has been a problem for the duration of the mission. There are currently few opportunities to determine, *post hoc*, the calibration of the radar at any given period, due to poor record keeping and numerous hardware failures. Based on our use of the 2002 base line KWAJ calibration, we are able to detect periods during which the relative calibration differed from the base line and are working to determine methodologies to apply these corrections for future version. Although the KPOL radar is dual-polarized, past quality of the data has been too poor to use for determining the absolute calibration, although we believe recent improvements to the radar may make use of data feasible for such purposes for current and future data. For past data, we are

currently investigating other techniques to provide unbiased estimates using the clutter detected during periods when there is little or no precipitation present. In 2002, the radar appears to have been relatively stable and without significant hardware and known calibration issues. For this reason, 2002 was selected for the WPMM yearly technique. It is noted that although the radar system appeared to be stable for this period, an absolute calibration offset might still need to be applied. Radar calibration fluctuations introduce a significant source of error into both instantaneous and monthly rain maps. The TRMM GV group is working to quantify and apply calibration offsets in such a manner that still allows independent evaluation/validation of TRMM satellite retrievals. One technique being considered is the application of a monthly radar-and-gauge determined bulk adjustment factor. The bulk-adjustment factor would shift the entire WPMM curve in log-log space without altering the slope, and would calibrate the $Z_e$ distribution to match R from the gauges. This method, of course, could not be used if there are no "good" gauges for a particular month. By using the 2002-based WPMM, we were able to detect periods during which the relative radar calibration was different than the 2002-baseline.

*c. Dependent versus Independent Validation*

In order to evaluate the monthly rainfall product over a given site, several different validation methods (dependent, quasi-independent, and independent) have been employed. In the dependent validation process, rain gauge data that were used to create the *R* distribution for the monthly WPMM $Z_e$-R are compared with radar rain rate accumulations. The resulting statistics from dependent validation are basically an

algorithm and technique sanity check. Figure 9 shows an example of dependent validation results at MELB for August 1998. QC'd rain gauge data (TSP 2A-56), which we assume to be the ground truth estimate of surface rainfall, are shown on the abscissa. Dependent validation (by definition) will result in a radar-to-gauge (R/G) ratio very close to unity (Table 5). For quasi-independent validation, if the number of gauges in a network is sufficient, a given percentage of the gauges can be randomly selected and isolated from the total set of gauges and then not used in the generation of the R distribution. We refer to this as a *quasi-independent* validation, as the initial set of data has been altered to a slight degree. In an independent validation, an entirely separate network of gauges exists for validation. In this case, the original data collection network remains intact. In the TRMM era, these conditions were met only over the MELB site during TEFLUN-B conducted in the summer of 1998. Independent validation was conducted by the TRMM GV group (also Habib and Krajewski, 2002), from TEFLUN-B. The existence of independent gauge networks for validation is an essential factor in the generation of dependable rainfall estimates.

*d. Selecting and Using Independent Gauges for Validation*

For MELB, August 1998 was a unique month in that a true independent validation of the TSP 3A-54 was possible. Independent validation of this specific monthly rain map is accomplished by validating against gauge data that were not used in $Z_e$-R development. The August 1998 results (Fig. 10) are based on data from 15 independent gauges that were installed in the Melbourne vicinity for the TEFLUN-B TRMM field campaign.

These 15 gauges were not used in the operational WPMM $Z_e$-R development. Table 5 shows an R/G bias of 1.08, or an 8% overestimation by the radar, and normalized mean absolute difference (MAD) of 0.09 for these data. The MAD is defined as the mean of the absolute differences between monthly gauge and radar accumulations. These monthly statistics fall within acceptable bounds and are consistent with the independent findings of Habib and Krajewski (2002). Amitai et al. (2001, 2002) point out that such a low MAD might be explained by the natural variability of rain and gauge instrumental errors, and based on further analysis of the same data set as in Fig. 10, they demonstrated (see their Fig. 1) that the difference in accumulations of the gauges located within the same radar pixel were of the same order as the MAD, suggesting that the radar accuracy may be higher, but a denser gauge network is required for verification.

True independent gauge data are not available every month or at every site, so a technique was devised for quasi-independent evaluation. Quasi-independent gauge data are obtained by withholding 10% of the dependent gauges from a particular month from the WPMM $Z_e$-R process. Gauges to be withheld are selected using a random number generator based on atmospheric noise (http://random.org). New $Z_e$-R lookup tables are developed and applied without these randomly selected gauges. The resulting monthly rainfall accumulation map is then compared directly with these withheld gauges. Technically, this method does not evaluate the official monthly rainfall product, however, significant changes to the $Z_e$-R distributions have not been noted due to the small percentage of gauges withheld.

Figure 11 shows the dependent validation from MELB for September 1998 and Fig.12 shows the quasi-independent validation results for that month. The dependent validation (Table 5) lists a radar-to-gauge ratio (R/G) of 1.01 (as expected), and a MAD of 0.14. Quasi-independent results using eight randomly withheld gauges from $Z_e$-R development (Fig. 12), show R/G of 0.93 and MAD of 0.12. Table 6 provides a 16-month summary of quasi-independent validation results from MELB. Relatively rainy months were chosen. The 16-month radar-to-gauge bias (SR/SG) is 1.004. MAD values range from 0.08 to 0.28. As explained in Amitai et al. (2001), the natural variability of rain (within the scale of a radar pixel) and gauge instrument errors may explain a major fraction of the MAD. Point measurements from gauges are not at the same scale of a radar pixel, so gauge-based probability distribution functions (PDF) of R, which are used as ground truth, may not be representative of the actual R distribution at the scale of a radar pixel (Amitai et al. 2002). It is difficult to address this issue, as sufficiently dense gauge networks necessary to represent the distribution of R at a radar pixel size are not available at TRMM GV sites. It may be feasible to apply this quasi-independent validation approach to additional validation sites, such as Houston and Darwin, and potentially new GV sites such as the Florida Keys (Wolff et al. 2003), and Wallops Island, Virginia. However, the quasi-independent validation approach just described should not be applied to the Kwajalein Atoll site due to the limited amount of "good" rain gauge data.

As was previously mentioned, the entire year of radar and rain gauge data from 2002 (except December) were used in developing the KWAJ $Z_e$ and R distributions for a

yearly-based WPMM $Z_e$-R to be applied to all months. Therefore, any gauges considered "good" from months other than from year 2002 can be considered independent and used for validation purposes. From December 1997 through December 2001, only 18 months out of a possible 49 months had statistics within acceptable bounds for reliable rainfall estimation and validation. Acceptable statistical bounds are subjectively defined in this study as follows: MAD<0.3, and R/G between 0.75 and 1.25. From these 18 months, R/G ratios ranged from 0.79 to 1.19, while the MAD varied from 0.11 to 0.27. For the dependent months (Jan-Nov 2002), R/G varied from 0.79 to 1.23, while the MAD varied from 0.12 to 0.25. Figure 13 shows an ensemble scatter-plot with the combined results of the 18 months with acceptable radar and gauge comparison statistics. All gauges used in this plot are considered independent. Additional scatter-plots and validation statistics are posted on the TRMM Satellite Validation Office web site (http://trmm-fc.gsfc.nasa.gov/trmm_gv).

*e. Comparison of Rain Estimates at KWAJ*

Both the TSVO and the Department of Atmospheric Sciences at the University of Washington (hereafter UWASH) have produced TRMM GV products at KWAJ. The methodologies used to produce these estimates vary slightly, but overall the results compare quite favorably with one another. The UWASH group uses a disdrometer-based Z-R to convert radar reflectivities into rain intensities. A description of their methodology is provided in Houze et al. (2004).

Here we will present a comparison of Level II (rain intensity) and Level III (monthly rainfall) for the TSVO and UWASH products. The purpose of this effort is to provide the community with an understanding of the relative magnitudes of rainfall over KWAJ, as well as to provide an estimate of the relative difference between the two approaches.

*f. Level II Comparisons*

The GV data from July through December 1999 were selected for comparison, based on the current availability of the UWASH products. This data set provided approximately 4500 rain intensity maps for comparison. Only time-coincident maps were compared. For each map, the conditional mean rain rate was computed; i.e. only points that were non-zero in both products were considered. Figure 14 provides scatter plots of these mean rain map values for each month. The two rain intensity estimates are well correlated (r=0.87). TSVO rain intensities average about 13% higher than the UWASH estimates over the period.

*g. Level III Comparisons*

For the Level III comparisons, the six monthly rainfall maps (TSP 3A54 and 3A54UW) were used. The conditional mean rain rate was computed for each map and Figure 15 provides a comparison between the TSVO and UWASH Level III estimates. The monthly rainfall estimates are perfectly correlated, but the TSVO estimates are about

8% higher than UWASH estimates. The difference of the ratios in Level II (13%) and Level III (8%) are probably due to differences in the accumulation algorithm used by the two groups. The main factor affecting the differing integration techniques is due to the presence of radar data gaps (periods when the radar was not operating).

*h. Comparison of radar estimates to gauge observations.*

Figure 16 is a scatter plot of TSVO and UWASH versus gauge observations. Recalling that UWASH uses a single time-independent disdrometer-based power-law $Z_e$-R relationship, and that TSVO uses a WPMM $Z_e$-R derived from data in 2002, the following can be stated: 1) both of the comparisons provide independent validation; 2) both are well correlated, with TSVO and UWASH correlations of 0.87 and 0.77, respectively; and, 3) the TSVO and UWASH estimates are approximately 18% and 25% low relative to the gauge observations, respectively. No attempt is made here to state which estimates might be closer to the "truth", given the limited quantity and quality of gauge data at KWAJ. It has been determined that the differences between the GSFC estimates and the gauge accumulations can be attributed to by a radar calibration of only 1 dB. Houze et al (2004) state that they applied a +6 dB correction to the KWAJ reflectivity data prior to conversion to rain rate, while TSVO applied only +5 dB. After application of the additional +1 dB to the TSVO reflectivities, the R/G ratio was increased from 0.87 to 0.97 and the mean absolute difference decreased from 0.21 to 0.18, both significant improvements.

## 5. Comparisons to TRMM Satellite Estimates

Finally, we provide a brief review of how well the GV estimates compare to TRMM satellite-retrieved estimates. We note that the TRMM data used in this analysis is from the Version 6a algorithms over the period January 2001 through April 2002 and do not represent the "official" Version 6 estimates. The TRMM Science Data and Information System (TSDIS) is currently processing the official products and thus they are not available for comparison at the time of this writing. From personal communication with the algorithm developers (Kummerow, Meneghini and Haddad), we do not believe that there will be significant changes in these comparisons for over ocean; however, there may be some significant differences in the comparisons over land and coast and thus must be addressed in future research.

For brevity, we provide comparisons of our GV estimates over KWAJ and MELB only. For this analysis, estimates from the TRMM gridded 3G68 product were used to compare to GV rain intensities. The 3G68 global product provides the average rain rate in 0.5° x 0.5° pixels for the TRMM Microwave Imager (TMI), Precipitation Radar (PR) and Combined (COM) algorithms. Each 3G68 pixel that lies over the respective GV sites were extracted and then compared to TRMM GV estimates obtained by de-resolving the 2 km x 2km 2A53 rain map pixels to the same grid as the 3G68 product. Thus, the comparison was pixel-matched in both time and space, removing sampling as a source of error in these comparisons.

The data from each site was sub-setted to provide comparisons over Land, Coast and Ocean. For KWAJ, there are no land or coast pixels, as it is considered solely oceanic. Fig. 17 provides the classifications of the various pixels for MELB. Only pixels that are fully occupied by ocean "O" and fully envelop a GV pixel were used for analysis. The bias, defined in Eq. 1, provides a bulk estimate of the agreement between GV and the satellite estimates. In Eq. 1, *Satellite* is the TRMM estimate (PR, TMI or COM) and *GV* is the GV.

$$Bias = \frac{Satellite - GV}{GV} \tag{1}$$

Calculating a "bulk" bias, using all 0.5° pixels in which there was at least one PR footprint and fully contained a valid GV region, the TRMM estimates match well with GV estimates over open ocean. For KWAJ (see Fig. 3a), the PR, TMI and COM estimates were +6%, -4.6% and +14% of GV estimates, respectively. For MELB (see Fig. 3b), the PR, TMI and COM estimates were –9.,1%, -5.7% and –2.4% of GV estimates, respectively. Thus a strong convergence is evident not only the TRMM satellite estimates, but also between TRMM and GV.

Over land and along the coastal areas, there are substantial differences between the various TRMM algorithms; however, it is our understanding that the official Version 6 products will mitigate some of these differences. Current research and future efforts will provide considerably more detail on the effectiveness of the GV estimates in

validating TRMM, but it suffices to say here that the latest products for GV and the satellite have converged to a point that have nearly achieved the early prognostications of 10% error over a 5° x 5° box on a monthly scale by North et al. (1986).

A detailed discussion on the regional and physical differences between the various TRMM algorithms is beyond the scope of this paper; however, work is underway now to provide similar validation on a satellite "footprint" scale in order to better understand why the apparent regional differences in the estimates occur (Kummerow, personal communication).

**6. Summary and Conclusions**

An overview of the Tropical Rainfall Measuring Mission (TRMM) Ground Validation Program is presented. The validation program is based at NASA Goddard Space Flight Center in Greenbelt, Maryland and is responsible for processing several TRMM science products for validation space-based rain estimates from the TRMM satellite. These products include gauge rain rates, radar rain intensity, precipitation type, and rain accumulations. The rain intensity estimates are derived using the Window Probability Matching Method (WPMM). WPMM matches the probabilities of radar observed reflectivities $Z_e$ and gauge measured rain intensity $R$ in such a way that the PDF of the radar estimated R above the gauge will be identical to the PDF of the gauge rates on a monthly scale. The resulting $Z_e$-R functions are curved lines in log-log space rather than a straight-line power law. A comparison of the NASA GV program products and

those developed by the University of Washington for a subset of data from one of the sites (Kwajalein, Republic of the Marshall Islands) is presented and it is shown that the two estimates are near 10% of one another on both instantaneous and monthly time scales. It is shown that, for the period July – December 1999, both the NASA and UWASH estimates are lower than the gauge-measured monthly rain totals by 18% and 25%, respectively. Finally, a brief comparison of NASA GV rain intensities to satellite retrievals from the TRMM Microwave Imager (TMI), Precipitation Radar (PR) and Combined (COM) algorithms is presented and it is shown that the GV and satellite estimates agree quite well over ocean. At Kwajalein, all three satellite estimates are well within 10% of GV estimates, while at Melbourne, Florida, both the TMI and PR are within 10% of GV estimates and the COM algorithm is approximately 14% higher than the GV estimates. Further research on the official Version 6 products will be conducted when that data becomes available some time in 2005.

*Acknowledgements*

The authors would like to thank Dr. Ramesh Kakar (NASA Headquarters), Dr. Robert Adler (TRMM Project Scientist) and Mr. Richard Lawrence (Chief, TRMM Satellite Validation Office) for their guidance and support of this effort. We also appreciate the support staff of the TSVO, including David Makofski, Bart Kelley, David Augustine, and Marcella Shupp.

REFERENCES

Amitai E., J. A. Nystuen, L. Liao, R. Meneghini, and E. Morin, 2004: Uniting space, ground and underwater measurements for improved estimates of rain rate. *IEEE Geoscience and Remote Sensing Letters*, **1**, No. 2, April, 2004.

Amitai E., D. B. Wolff, D. A. Marks, and D. S. Silberstein, 2002: Radar rainfall estimation: Lessons learned from the NASA/TRMM validation program. *Second European Conference on Radar Meteorology (ERAD),* November 18-22, Delft, The Netherlands. ERAD Publication Series, **1**, 255-260 (Copernicus, ISBN 3-936586-04-7).

Amitai E., D. B. Wolff, M. Robinson, D. S. Silberstein, D. A. Marks, M. S. Kulie, and B. Fisher, 2001: Methodologies for evaluating the accuracy of TRMM ground validation rainfall products. Preprints, *30th Int. Conf. on Radar Meteorology,* July 19-25, Munich, Germany, AMS, 363-365.

Amitai, E., 2000: Systematic variation of observed radar reflectivity-rainfall rate relations in the tropics. *J. Appl. Meteor.* (Special Issue on TRMM), **39**, 2198-2208.

Anagnostou, Emmanouil N., C. A. Morales, T. Dinku, 2001: The Use of TRMM Precipitation Radar Observations in Determining Ground Radar Calibration Biases. *J. Atmos. Oceanic Technol.*: **18**, No. 4, pp. 616–628.

Atlas, D., D. Rosenfeld, and A. R. Jameson, 1997: Evolution of radar rainfall measurements: Steps and mis-steps. *Weather Radar Technology for Water Resources Management*, B. Braga and O. Massambani, Eds., UNESCO, 1-60.

Atlas, D, 1987: Early foundations of the measurement of rainfall by radar. Radar in meteorology: Battan Memorial and 40th Anniversary Radar Meteorology Conference (1987: Boston, Mass.) D. Atlas, Ed., AMS 86-97.

Austin, P. M., 1987: Relation between measured radar reflectivity and surface rainfall. *Mon. Wea. Rev.*, **115**, 1053-1070.

Ciach, Grzegorz J., Krajewski, Witold F., Anagnostou, Emmanouil N., Baeck, Mary L., Smith, James A., McCollum, Jeffrey R., Kruger, Anton. 1997: Radar rainfall estimation for ground validation studies of the Tropical Rainfall Measuring Mission. *Jou. App. Met.*, **36**, No. 6, 735–747.

Crum, T.D., R. L. Alberty, and D. W. Burgess, 1993: Recording, archiving, and using WSR-88D data. *Bull. Amer. Meteor. Soc.*, **74**, 645-653.

Doviak, R.J., 1983: A survey of radar rain measurement techniques. *J. Climate Appl. Meteor.*, ***22***. 832-849.

Gray. W., and R. W. Jacobson, 1977: Diurnal variation of deep cumulus convection. *Mon. Wea. Rev.,* **105**, 1171-1188.

Habib, E., and W. F. Krajewski, 2002: Uncertainty analysis of the TRMM ground-validation radar-rainfall products: Application to the TEFLUN-B field campaign. *J. Appl. Meteor.*, **41**, 558 572.

Habib, E., W. F. Krajewski, and A. Kruger, 2001: Sampling errors of tipping-bucket rain gauge measurements. *J. Hydrol. Eng.*, **6**, 159 166.

Hendon, H. H., and K. Woodberry, 1993: The diurnal cycle of tropical convection. *J. Geophys. Res.*, **98**, 16623-16637.

Houze, R. A., S. Brodzik, C. Schumacher, S. E. Yuter, 2004: The multi-year quantitative dataset produced by the Kwajalein Ground Validation Radar during TRMM. *J. Appl. Meteor., submitted.*

Keenan, T., Glasson, K., Cummings, F., Bird, T.S., Keeler, J., and Lutz, J., 1998: The BMRC/NCAR C-band polarimetric (C-POL) radar system. *J. Atmos. Oceanic Technol., **15**,* 871-886.

Keenan, T. D., R. E. Carbone, 1992: A preliminary morphology of precipitation systems in tropical northern Australia. *Quart. J. Roy. Met. Soc.,* **118**, pp. 283-326.

Keenan, T., and co-authors, 2000: The Maritime Continent Thunderstorm Experiment (MCTEX): Overview and Some Results**.** *Bull. Amer. Met. Soc.* Vol. **81**, No. 10, pp. 2433–2455.

Kraus, E. B., 1963: The diurnal precipitation over the sea. *J. Atmos. Sci.*, **20**, 551-556.

Kulie, M. S., Robinson, M., Marks, D.A., Ferrier, B.S., Rosenfeld, D., and Wolff, D.B., 1999: Operational processing of ground validation data for the Tropical Rainfall Measuring Mission. Preprints, *29th International Conference on Radar Meteorology*, July 12-16, Montreal, Canada, AMS, 736-739.

Kummerow, C., Barnes, W., Kozu, T., Shiue, J., and Simpson, J., 1998: The Tropical Rainfall Measuring Mission (TRMM) sensor package. *J. Atmos. Oceanic Technol.*, *15*, 809-817.

Marks, D.A., M. S. Kulie, M. Robinson, D.S. Silberstein, D. B. Wolff, B. S. Ferrier, E. Amitai, B. Fisher, J. Wang, D. and O. Thiele , 2000: Climatological processing and product development for the TRMM Ground Validation program. Physics and Chemistry of the Earth, (PCE), Part B: Hydrology, Oceans and Atmosphere, 25, 871-876.

North, G. R., 1987: Sampling studies for satellite estimate of rain. *Preprint Vol. Tenth Conference on Probability and Statistics in Atmospheric Sciences,* Amer. Met. Soc., Edmonton, Alberta, Canada, 129-135.

Rosenfeld, D., D. Atlas and D. B. Wolff and E. Amitai, 1992: Beamwidth effects on Z-R relations and area integrated rainfall. *J. Appl. Meteor.*, **32**, No. 1, 50-72.

Rosenfeld, D., D. B. Wolff, and E. Amitai, 1994: The window probability matching method for rainfall measurements with radar. *J. Appl. Meteor.*, 33, 682-693.

Schumacher, C., and R. A. Houze, Jr., 2000: Comparison of radar data from TRMM satellite and Kwajalein oceanic validation site. *J. Appl. Meteor.*, **39**, 2151-2164.

Simpson, J., Kummerow, C., Tao, W.-K., and Adler, R.F., 1996: On the Tropical Rainfall Measuring Mission (TRMM). *Meteor. Atmos. Phys.*, *60*, 19-36.

Steiner, M., Houze, Jr., R.A., and Yuter, S.E., 1995: Climatological characterization of three-dimensional storm structure from operational radar and rain gauge data. *J. Appl. Meteor.*, *34*, 1978-2007.

Wilson, J.W., and Brandes, E.A., 1979: Radar measurement of rainfall—A summary. *Bull. Amer. Meteor. Soc.*, *60*, 1048-1058.

Wolff, D. B., J. Gerlach, B. Fisher, A. Tokay, D. A. Marks, D. S. Silberstein, and J. Wang, 2003: On the characteristics of precipitation in the Florida Keys: The Keys

Area Precipitation Project. Preprints, *31st International Conference on Radar Meteorology*, Seattle WA, AMS 437-440.

Wolff, D. B., B. L. Fisher, O. W. Thiele and D. Han, 1995: Diurnal cycle of tropical rainfall based on rain gauge data: Implications for Satellite Rainfall Retrievals. *27th Conference on Radar Meteorology*. Vail, Colorado. October 9-13, 1995.

List of Figures

Fig. 1: Global map showing locations of the four TRMM GV sites: DARW (Darwin, Australia; HSTN (Houston, Texas); KWAJ (Kwajalein, RMI); and, MELB (Melbourne, FL).

Fig. 2: Average mean monthly rainfall in mm for the four GV sites. These averages were computed using five years of available GV-sponsored gauge data from the period 1998-2002. The average annual rain accumulation are shown in parentheses in the plot legend. Note that these values may differ from the climatological mean as they are derived from TRMM gauge data on not climatological records.

Fig. 3: Diurnal cycle of precipitation as expressed by the probability of occurrence of precipitation for a given hour (local time) at each of the four TRMM GV sites. These statistics were derived from five years of available GV-sponsored gauge data from the period 1998-2002.

Fig. 4: Map of the two rain gauge networks (KWA & RMI) deployed at the Kwajalein TRMM GV site. KWA network gauges are shown as black. The KPOL S-band radar is located on Kwajalein Island at the center of the figure

Fig. 5: Map of the three rain gauge networks (KSC: Kennedy Space Center; SFL: South Florida Water Management District; and STJ: St. John's River Water Management District) deployed at the Melbourne, Florida TRMM GV site. The three networks are

denoted as circles, squares, and triangles, respectively. KSC network gauges are located on Cape Canaveral, approximately 50 km NE of the KMLB WSR-88D radar (center). A Dense Rain Gauge Network (DRGN, not shown) is located approximately 40 km West of the radar.

Fig. 6: Map of the Harris County (HAR) rain gauge network deployed at the Houston, Texas TRMM GV site. Most HAR gauges are located to the northwest of the KHGX WSR-88D radar (center).

Fig. 7: Map of the CSC rain gauge network deployed at the Darwin, Australia TRMM GV site. Other higher-scale networks are available, but not shown. The Darwin C-band polarimetric (CPOL) radar is located at the center of the figure.

Fig. 8: Flowchart of TRMM GV data processing, quality control, and product generation. TRMM Standard Products (TSP) are indicated by darkened ovals and are defined in the text. Algorithms or programs are represented by rectangles, and lighter ovals represent intermediate files created in the $Z_e$-R table generation.

Fig. 9: Evaluation of August, 1998 monthly rain accumulations against dependent rain gauge data (i.e. gauge data shown were used in the development of the applied monthly WPMM $Z_e$-R lookup tables) from the Melbourne, Florida GV site. Each symbol represents a monthly accumulation (in mm) from the rain gauge (2A-56) and radar estimate above the gauge (3A-54).

Fig. 10: Same as Fig. 9, except that the gauges plotted were not used in determination of the $Z_e$-R algorithm and thus provide independent validation of the radar estimates.

Fig. 11: Same as Fig. 9, except that the period of coverage is for September 1998.

Fig. 12: Same as Fig. 9, except for quasi-independent gauges (i.e., sub-set of gauges are removed from the population of regular gauges prior to development of the $Z_e$-R relations.

Fig. 13: Sixteen-month ensemble validation results from the Kwajalein Atoll GV site. The WPMM $Z_e$-R lookup table was derived from 2002 data (see text); therefore gauge data from years other than 2002 are being considered independent. The 16-month period (which resulted in 90 radar and gauge plotting points) is from data prior to year 2002.

Fig. 14: Scatter-plot illustrating a comparison between TSVO and UWASH mean rain rates for the KWAJ radar. Each point represents the mean rate of a given instantaneous rain map from the two products. There are approximately 144 rain maps observed each day, and the plot shown covers all such rain maps produced for the period July 1 – December 31, 1999. Also shown is the regression equation between the two estimates as well as their correlation.

Fig. 15: Scatter-plot illustrating a comparison between TSVO and UWASH mean monthly rainfall for the KWAJ radar. Each point represents the mean rate of a given monthly rain map from the two products. The plot shown covers the period of July 1 –

December 31, 1999. Also shown is the regression equation between the two estimates as well as their correlation.

Fig. 16: Scatter-plot of TSVO and UWASH monthly rainfall estimates above gauges versus the observed rainfall by those gauges. Also shown are the respective regression equations and correlations.

Fig. 17: Mask used for comparing TRMM and GV instantaneous rates. Each pixel is a 0.5° x 0.5° box: "L" represents land; "C" represents coast; "O" represents ocean; "P" represents pixels that contain more than one distinct geographical type (L, C or O) and "F" represents pixels that contain only one geographical type and are fully within the radar domain (i.e. less than 150 km).

Fig. 18: Bias of TRMM satellite estimates relative to GV for the period Jan. 2001 through Apr. 2002 for a) KWAJ and b) MELB. These biases are calculated by comparing the mean rain rate over 0.5° x 0.5° pixels in the GV domain. Only pixels that were considered as "ocean" by the TRMM satellite algorithms are shown. The bias is defined as the difference between the GV and satellite and GV mean for the period, normalized to the GV mean and is expressed in Eq. 1 in the text.

List of Tables

Table 1: Characteristics of the Kwajalein (KPOL) radar located on Kwajalein Island at the southern tip of Kwajalein Atoll in the Republic of the Marshall Islands.

Table 2: Task configuration for KPOL radar. Columns are: task name, radar polarization, azimuth sweep rate in deg s-1, elevation angles in degrees, pulse repetition frequency (PRF), and run time in minutes and seconds.

Table 3: Description of the available networks, number of locations, gauge types and tipping-bucket rain increment for the four TRMM GV sites.

Table 4: Description of the primary TRMM Standard Products (TSP) produced for Ground Validation.

Table 5: Results of Validation comparisons between gauge-measured monthly rainfall and those of WPMM radar estimates. There are three types of validation: 1) IND: fully independent, in which gauges that are used for validation are not used for determination of the WPMM probabilities; 2) DEP: dependent, in which gauges that are used for determination of the calibration are also used for validation; and, 3) QUA: quasi-independent, in which a subset of the total number of gauges are excluded in the determination of the WPMM probabilities, but then are used for validation (see text for further details). Also shown are the periods over which the validations are made, the mean rainfall of the gauges and radar estimates, as well as the bias, relative to the gauge

mean, expressed in percent, and the Mean Absolute Difference (MAD), defined as the mean absolute difference between the gauge and radar rain totals.

Table 6: Quasi-Independent Monthly Validation for Melbourne, Florida. Shown are the month and year, radar to gauge ratio, mean absolute deviation and the number of gauges that were used to derive the statistics.

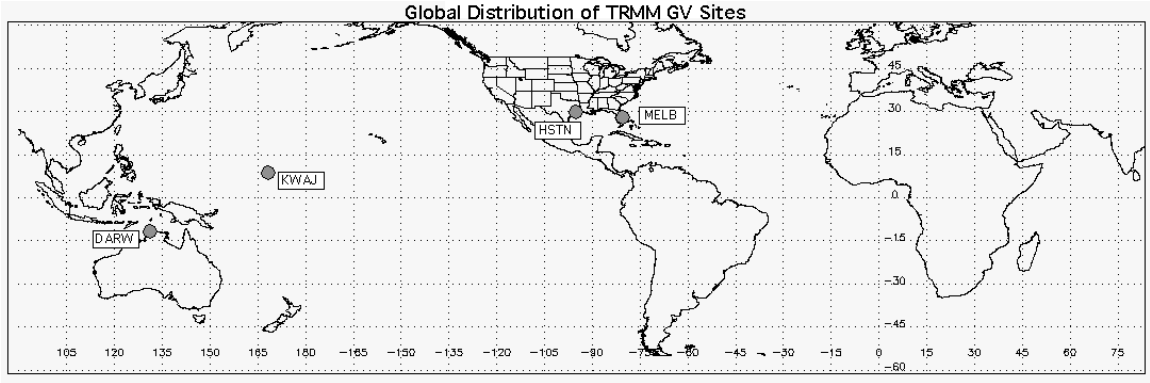


Fig. 1: Global map showing locations of the four TRMM GV sites: DARW (Darwin, Australia; HSTN (Houston, Texas); KWAJ (Kwajalein, RMI); and, MELB (Melbourne, FL).

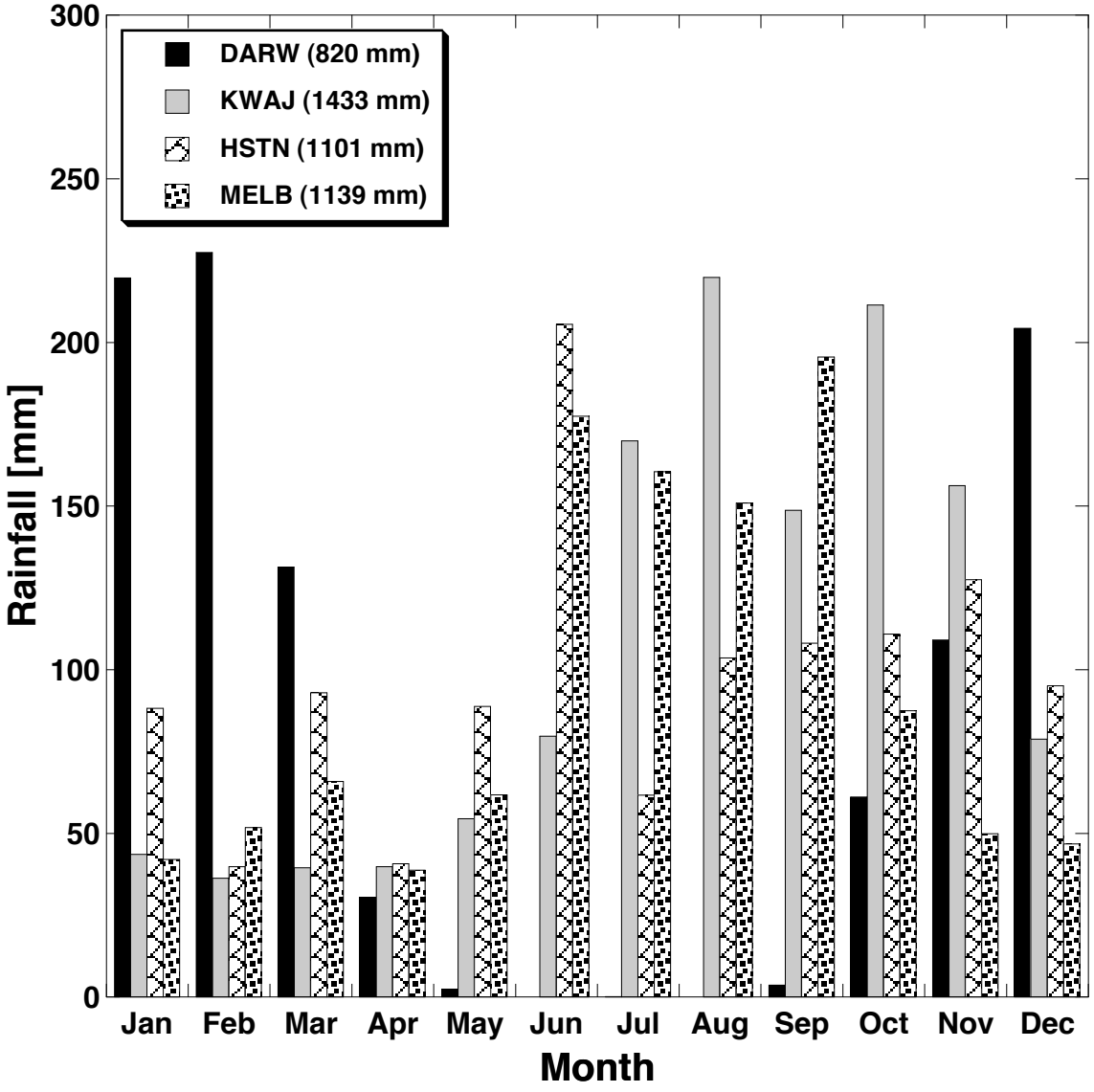


Fig. 2: Average mean monthly rainfall in mm for the four GV sites. These averages were computed using five years of available GV-sponsored gauge data from the period 1998-2002. The average annual rain accumulation are shown in parentheses in the plot legend. Note that these values may differ from the climatological mean as they are derived from TRMM gauge data on not climatological records.

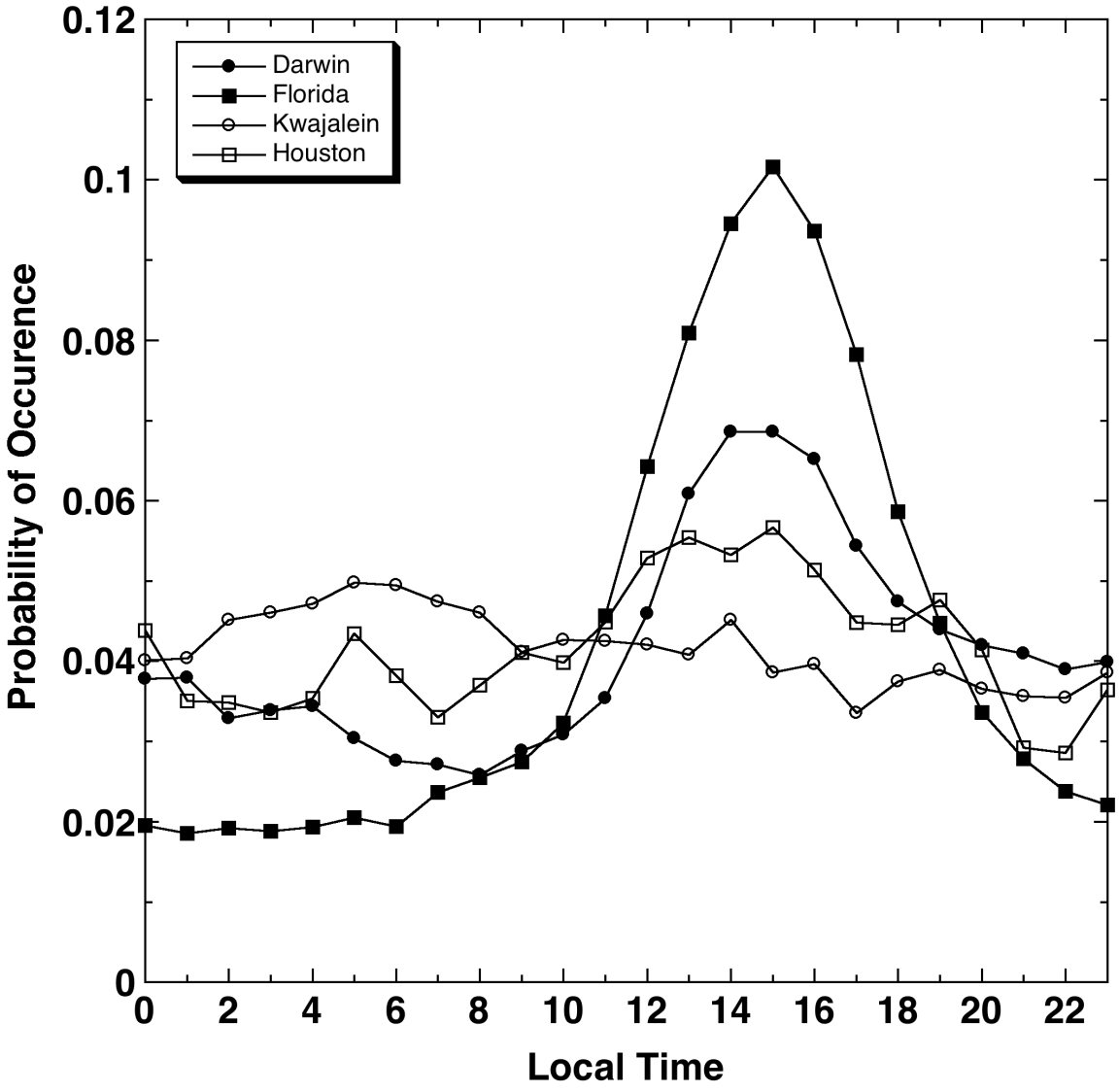


Fig. 3: Diurnal cycle of precipitation as expressed by the probability of occurrence of precipitation for a given hour (local time) at each of the four TRMM GV sites. These statistics were derived from five years of available GV-sponsored gauge data from the period 1998-2002.

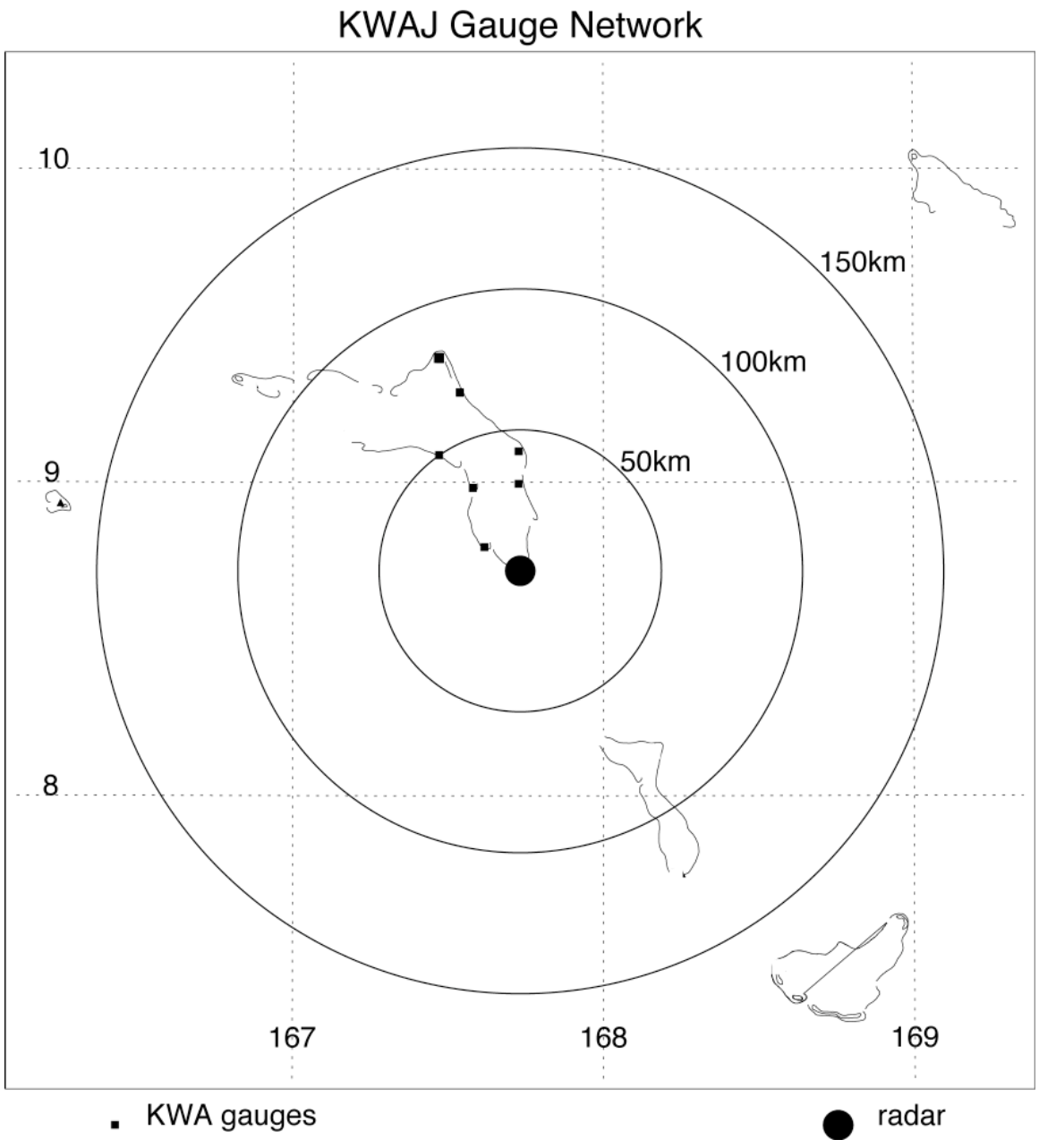


Fig. 4: Map of the two rain gauge networks (KWA & RMI) deployed at the Kwajalein TRMM GV site. KWA network gauges are shown as black. The KPOL S-band radar is located on Kwajalein Island at the center of the figure

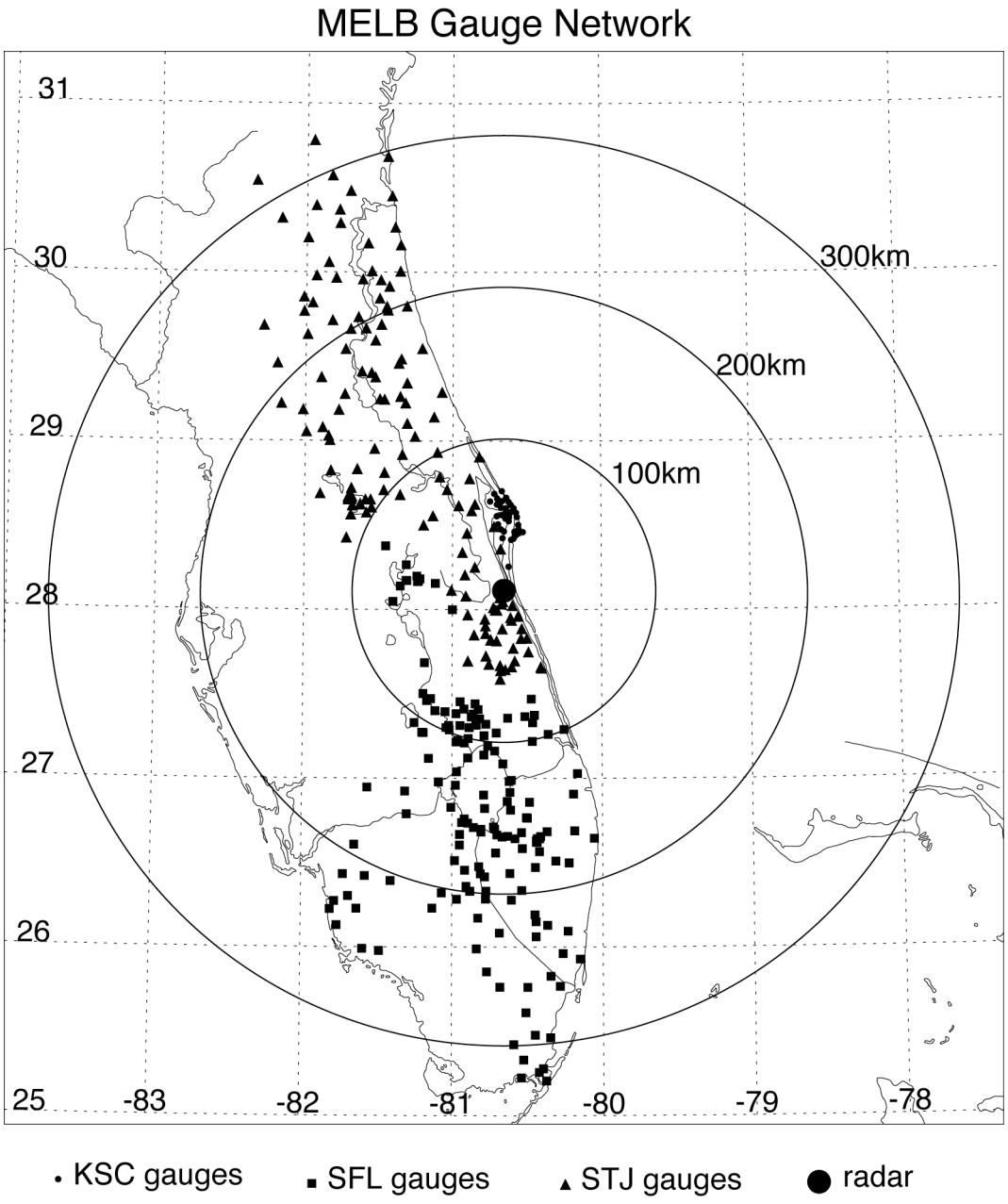


Fig. 5: Map of the three rain gauge networks (KSC: Kennedy Space Center; SFL: South Florida Water Management District; and STJ: St. John's River Water Management District) deployed at the Melbourne, Florida TRMM GV site. The three networks are denoted as circles, squares, and triangles, respectively. KSC network gauges are located

on Cape Canaveral, approximately 50 km NE of the KMLB WSR-88D radar (center). A Dense Rain Gauge Network (DRGN, not shown) is located approximately 40 km West of the radar.

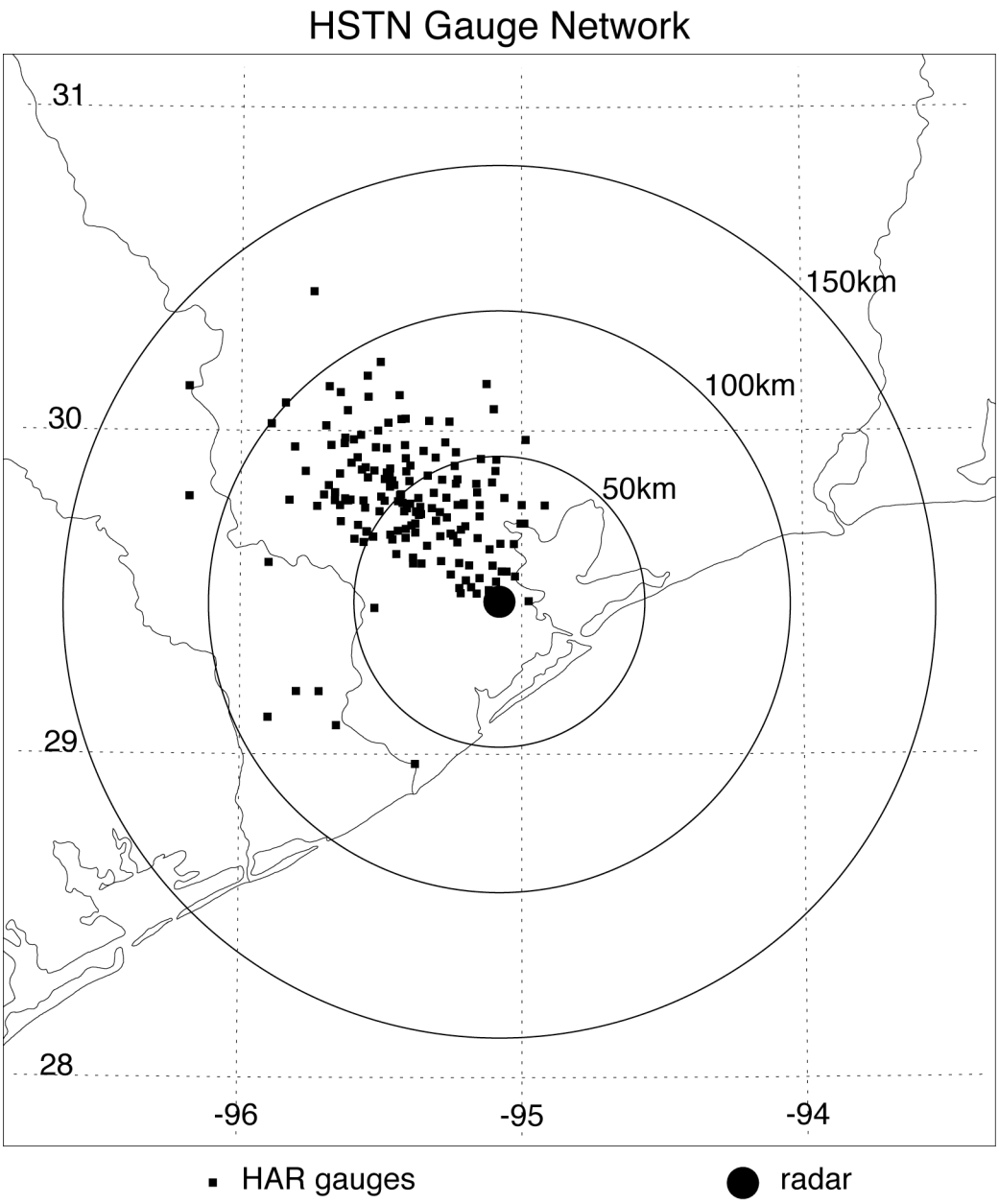


Fig. 6: Map of the Harris County (HAR) rain gauge network deployed at the Houston, Texas TRMM GV site. Most HAR gauges are located to the northwest of the KHGX WSR-88D radar (center).

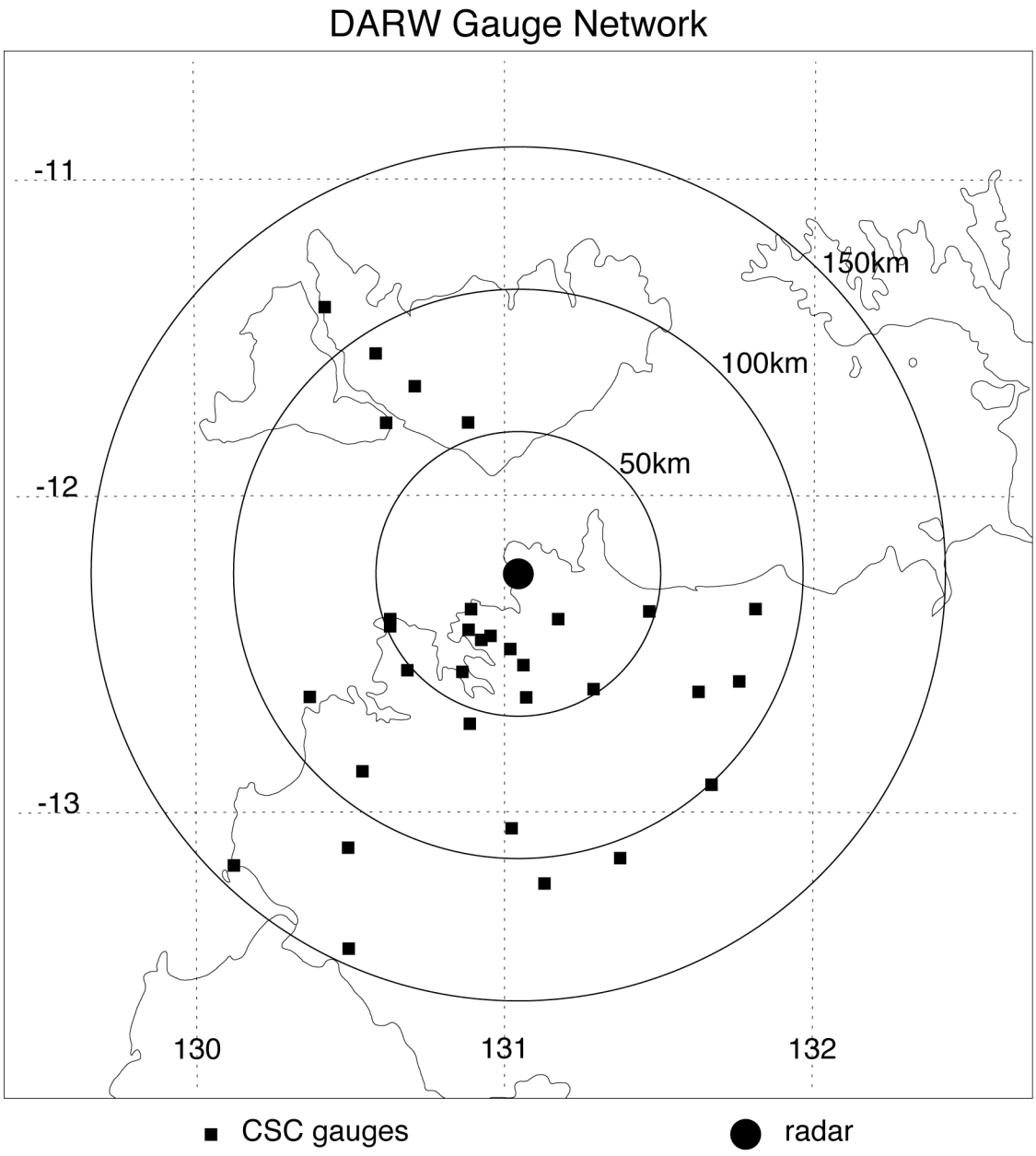


Fig. 7: Map of the CSC rain gauge network deployed at the Darwin, Australia TRMM GV site. Other higher-scale networks are available, but not shown. The Darwin C-band polarimetric (CPOL) radar is located at the center of the figure.

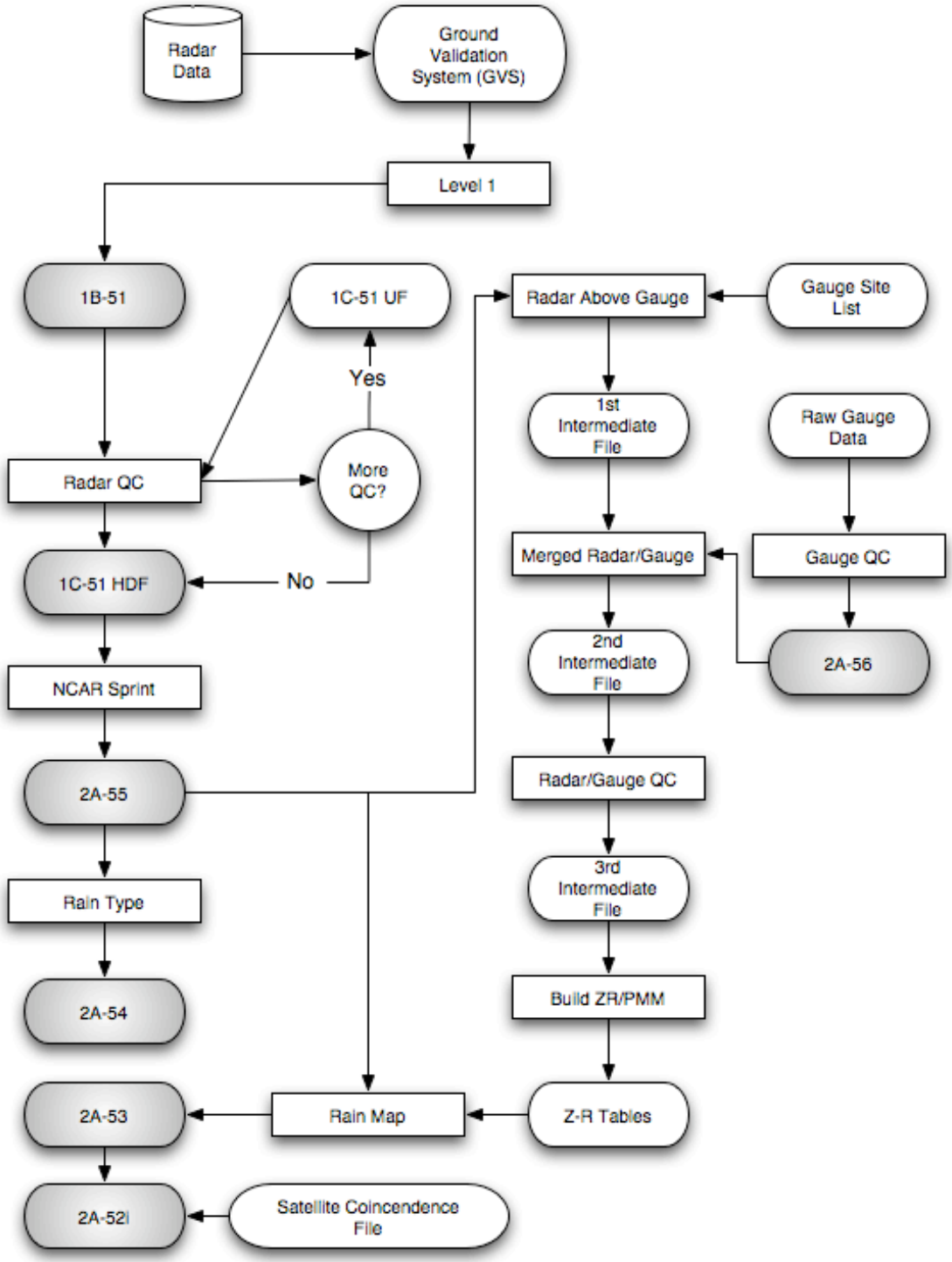


Fig. 8: Flowchart of TRMM GV data processing, quality control, and product generation. TRMM Standard Products (TSP) are indicated by darkened ovals and are

defined in the text. Algorithms or programs are represented by rectangles, and lighter ovals represent intermediate files created in the $Z_e$-R table generation.

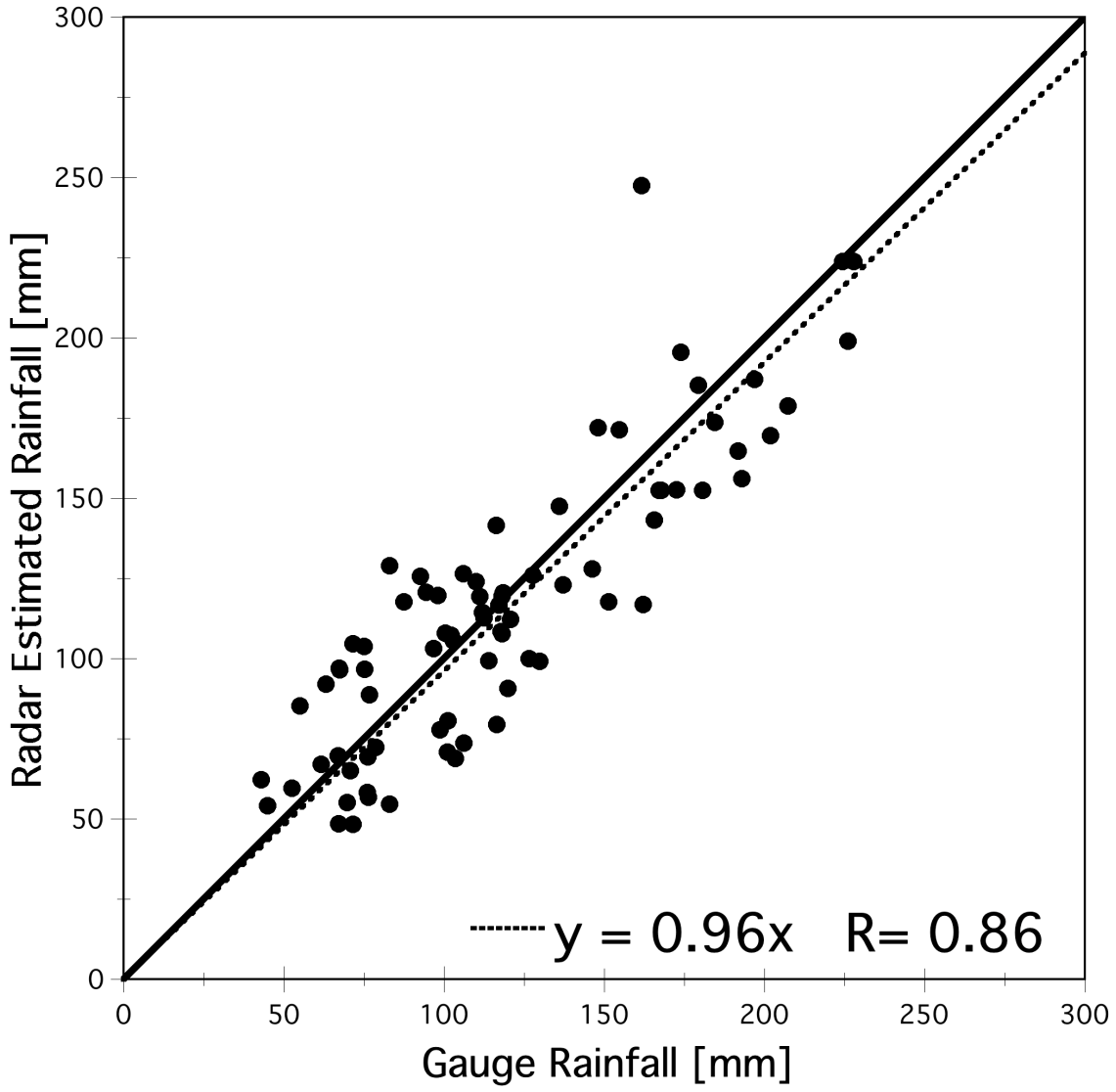


Fig. 9: Evaluation of August, 1998 monthly rain accumulations against dependent rain gauge data (i.e. gauge data shown were used in the development of the applied monthly WPMM $Z_e$-R lookup tables) from the Melbourne, Florida GV site. Each symbol represents a monthly accumulation (in mm) from the rain gauge (2A-56) and radar estimate above the gauge (3A-54).

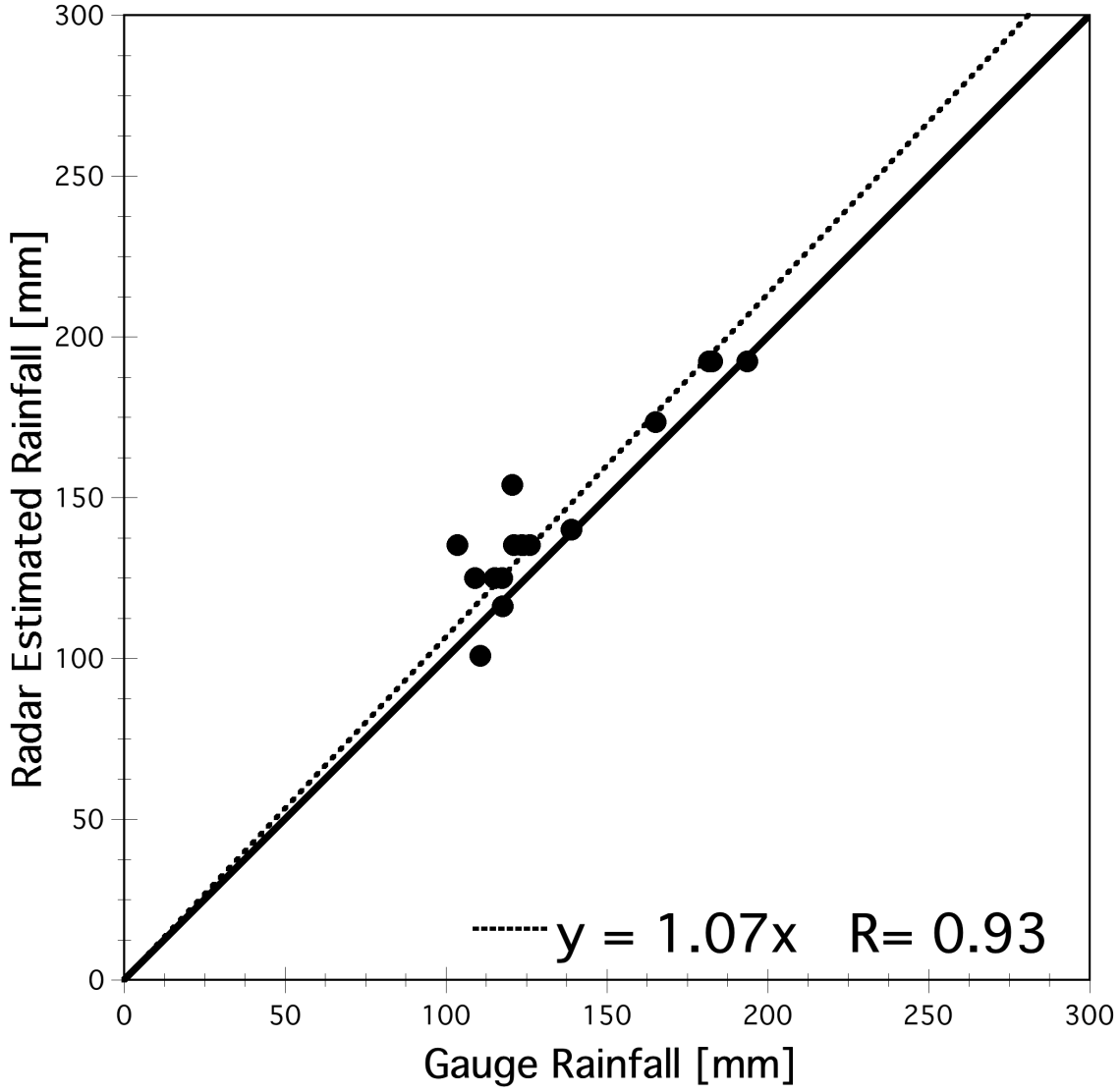


Fig. 10: Same as Fig. 9, except that the gauges plotted were not used in determination of the $Z_e$-R algorithm and thus provide independent validation of the radar estimates.

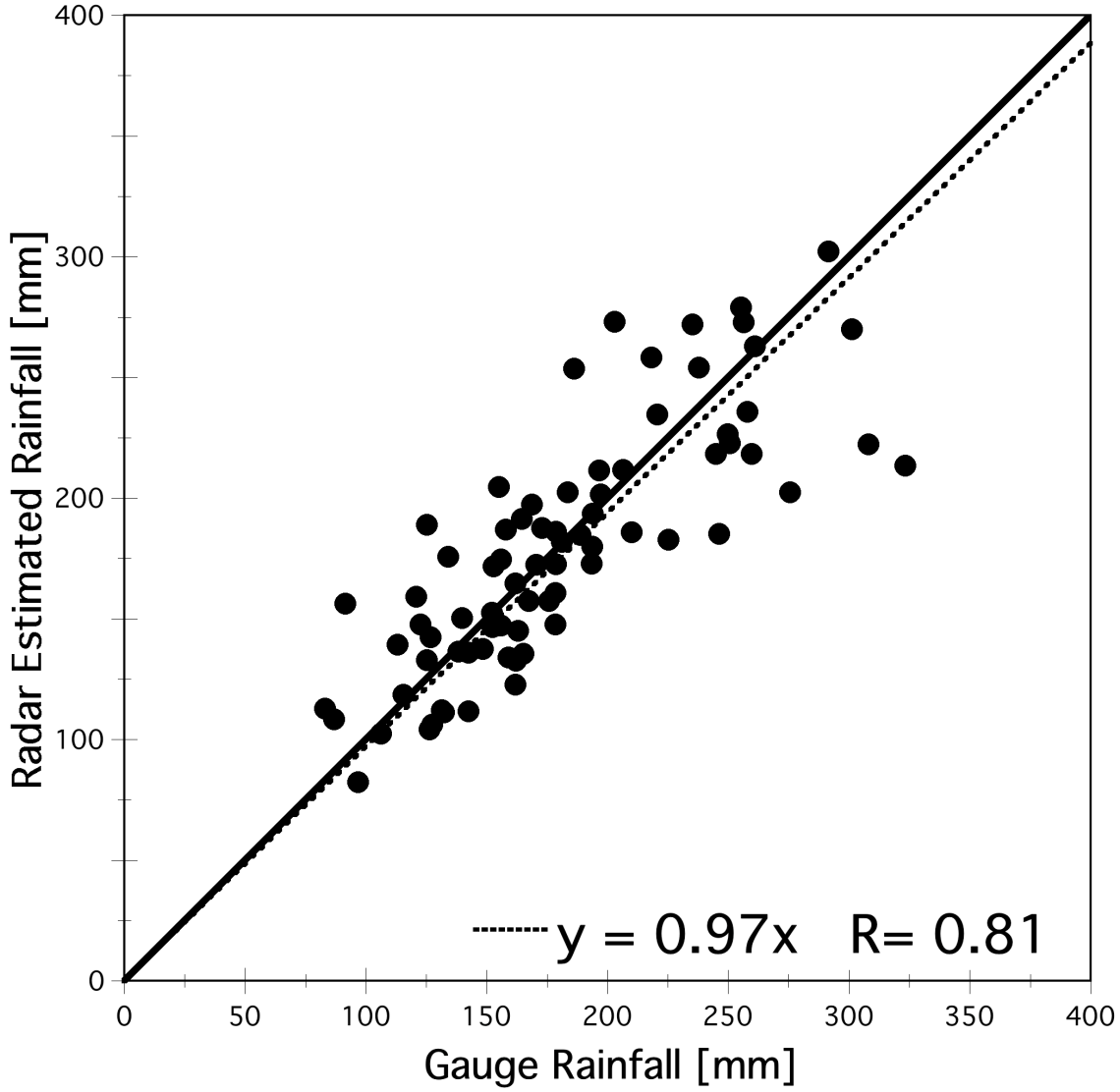

Fig. 11: Same as Fig. 9, except that the period of coverage is for September 1998.

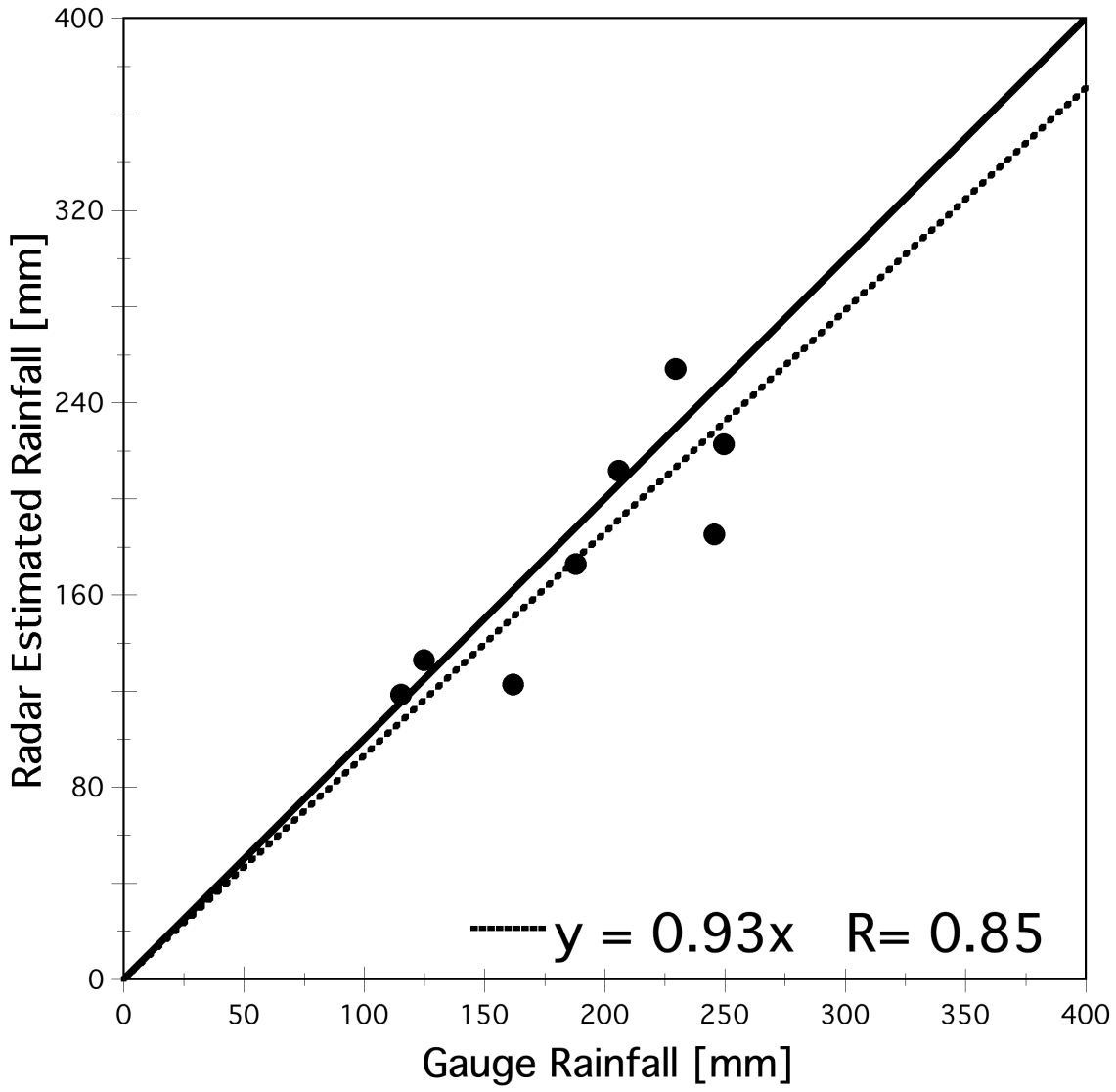


Fig. 12: Same as Fig. 9, except for quasi-independent gauges (i.e., sub-set of gauges are removed from the population of regular gauges prior to development of the $Z_e$-R relations.

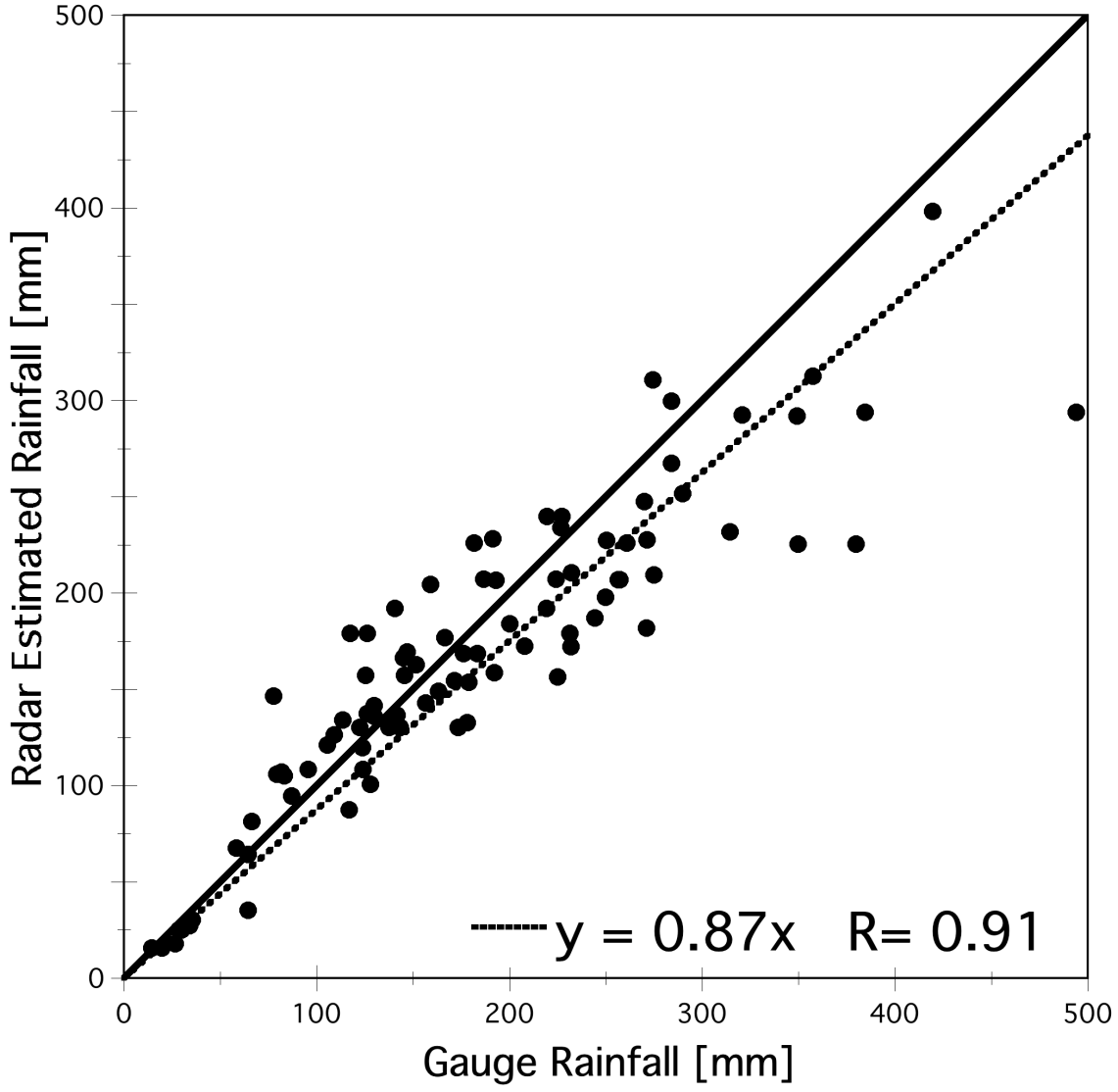


Fig. 13: Sixteen-month ensemble validation results from the Kwajalein Atoll GV site. The WPMM $Z_e$-R lookup table was derived from 2002 data (see text); therefore gauge data from years other than 2002 are being considered independent. The 16-month period (which resulted in 90 radar and gauge plotting points) is from data prior to year 2002.

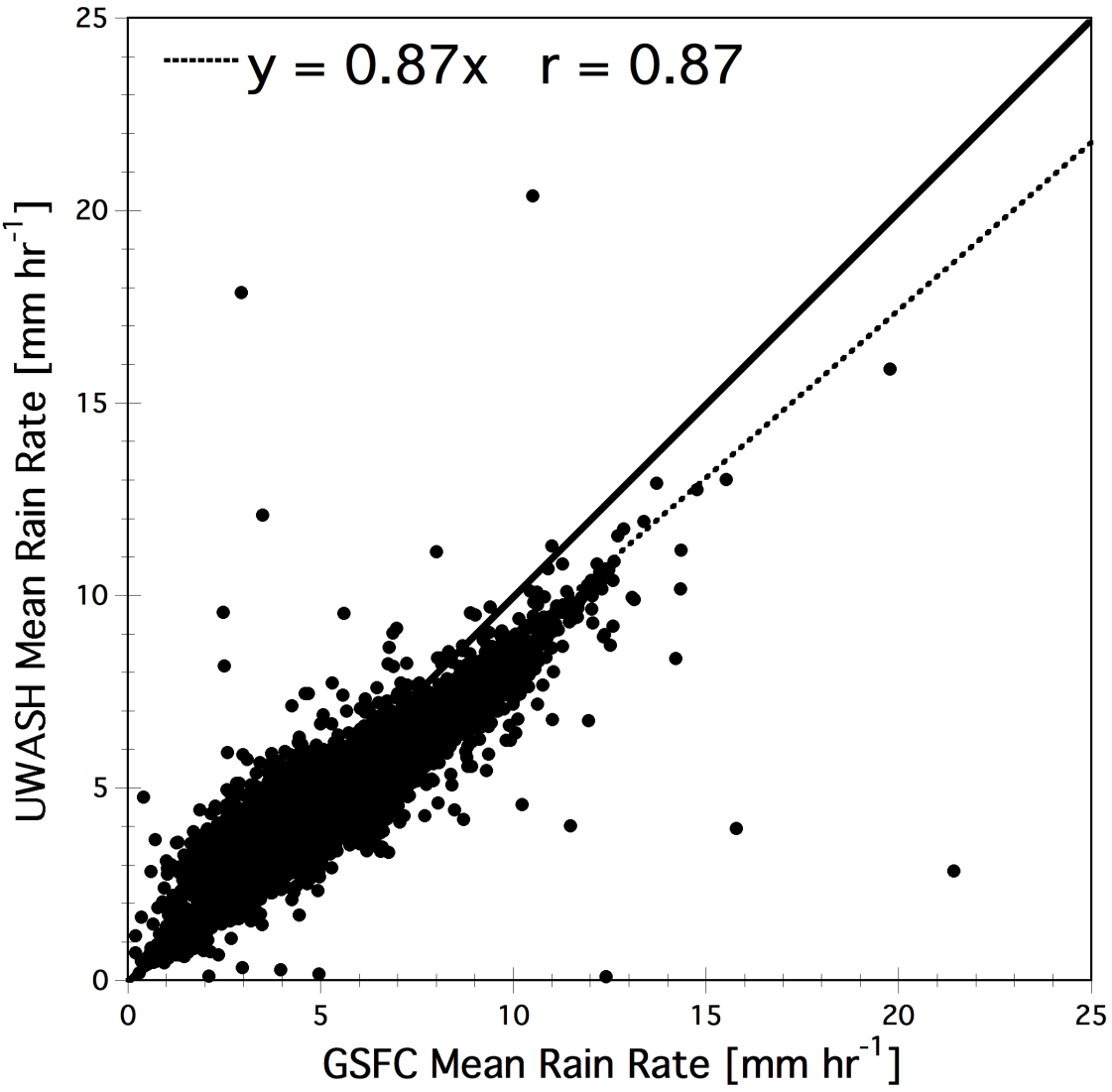


Fig. 14: Scatter-plot illustrating a comparison between TSVO and UWASH mean rain rates for the KWAJ radar. Each point represents the mean rate of a given instantaneous rain map from the two products. There are approximately 144 rain maps observed each day, and the plot shown covers all such rain maps produced for the period July 1 – December 31, 1999. Also shown is the regression equation between the two estimates as well as their correlation.

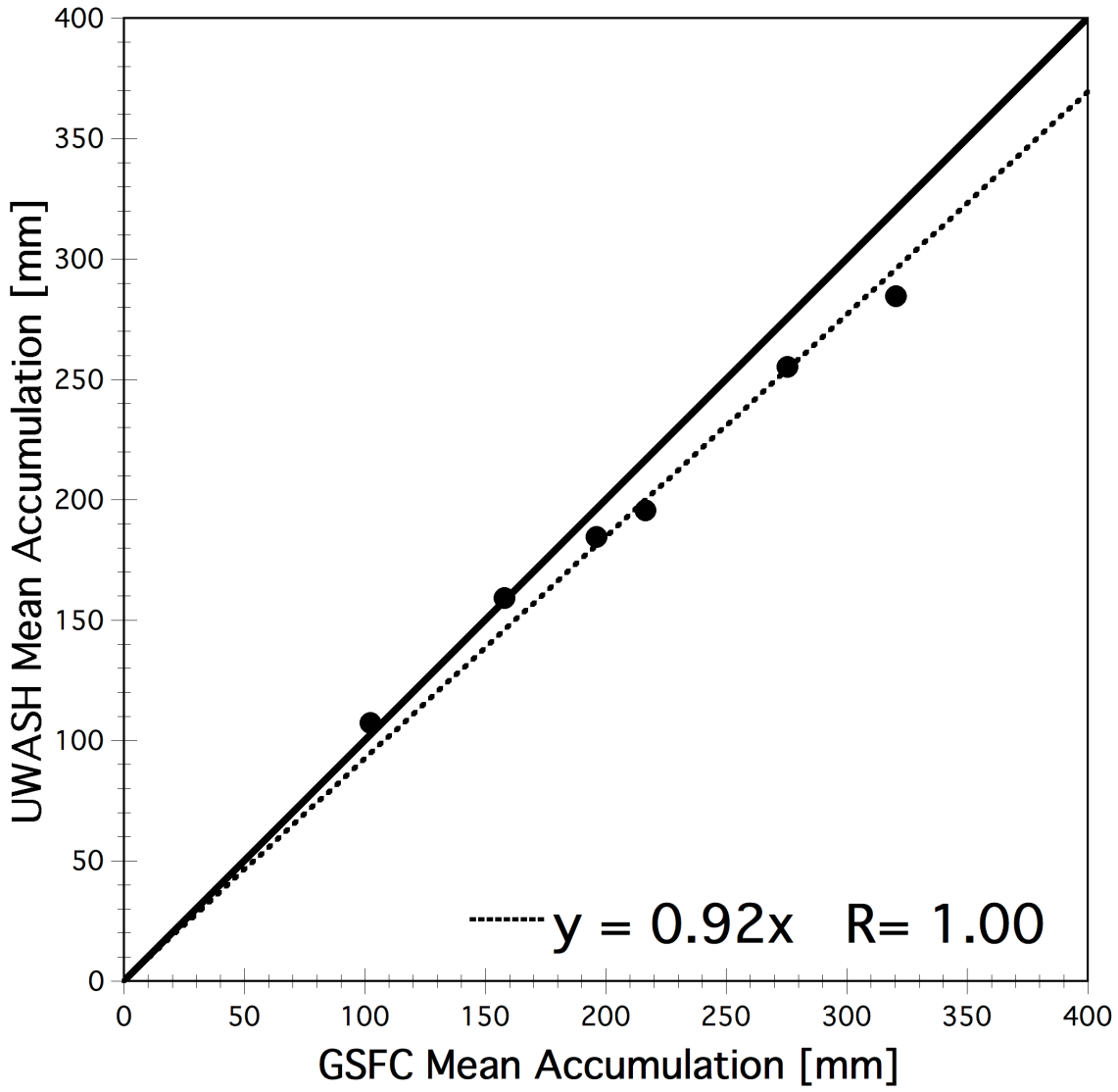


Fig. 15: Scatter-plot illustrating a comparison between TSVO and UWASH mean monthly rainfall for the KWAJ radar. Each point represents the mean rate of a given monthly rain map from the two products. The plot shown covers the period of July 1 – December 31, 1999. Also shown is the regression equation between the two estimates as well as their correlation.

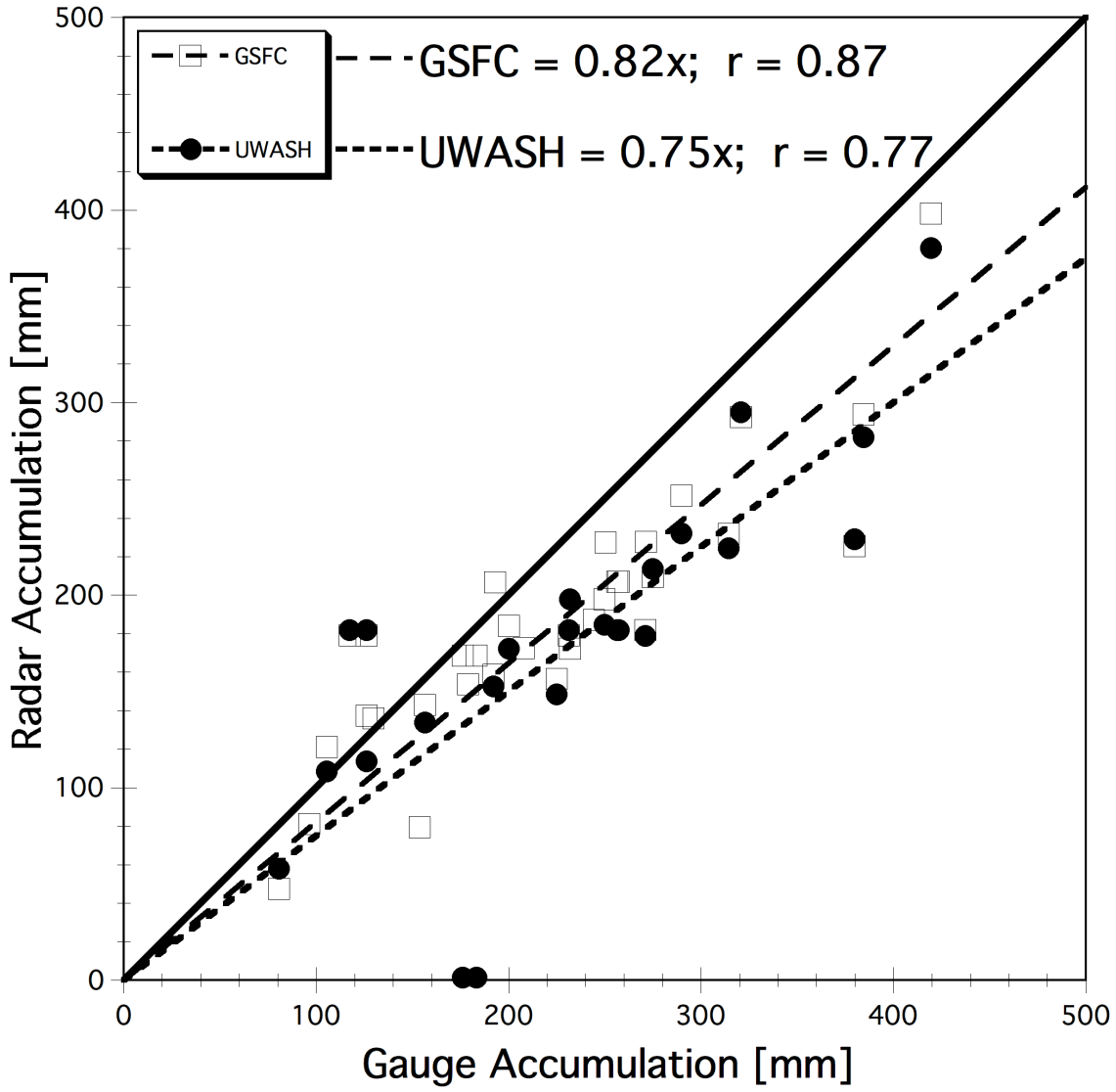


Fig. 16: Scatter-plot of TSVO and UWASH monthly rainfall estimates above gauges versus the observed rainfall by those gauges. Also shown are the respective regression equations and correlations.

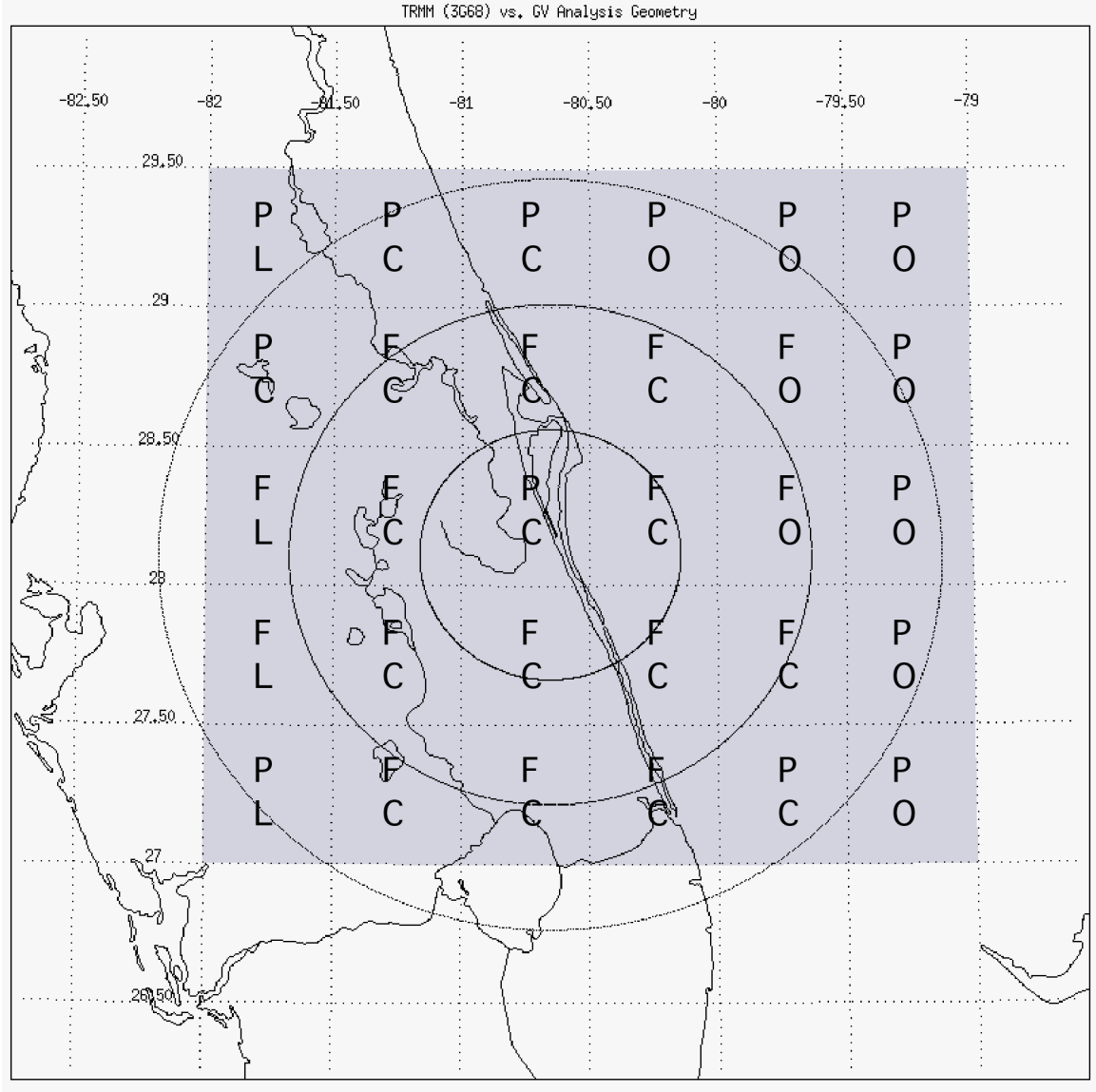


Fig. 17: Mask used for comparing TRMM and GV instantaneous rates. Each pixel is a 0.5° x 0.5° box: “L” represents land; “C” represents coast; “O” represents ocean; “P” represents pixels that contain more than one distinct geographical type (L, C or O) and “F” represents pixels that contain only one geographical type and are fully within the radar domain (i.e. less than 150 km).

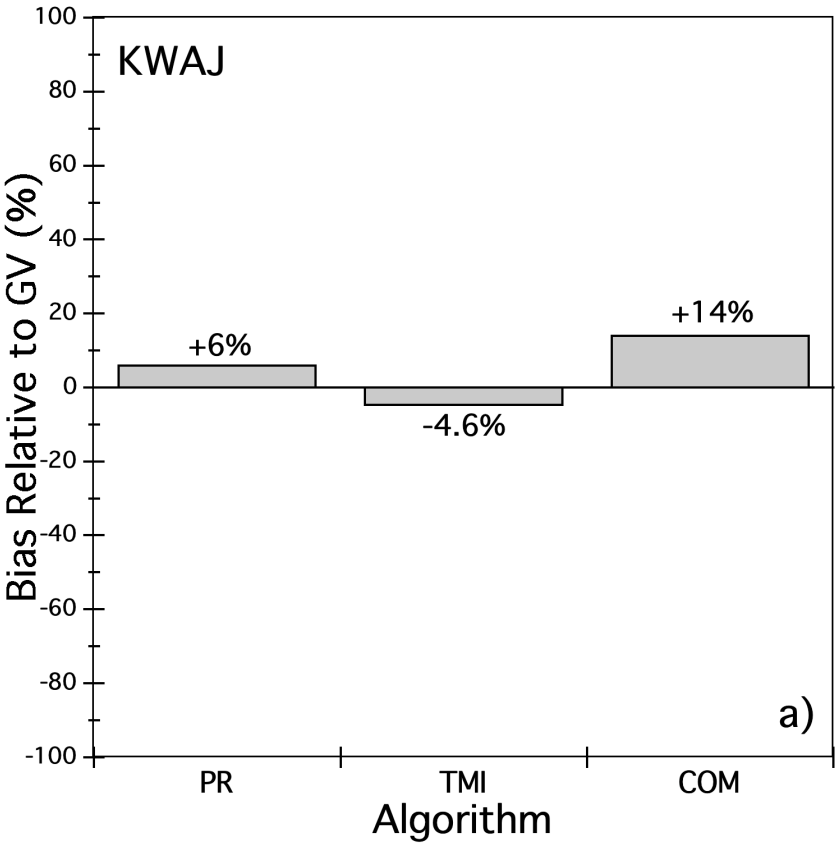
KWAJ
Bias Relative to GV (%)
100
80
60
40
20
0
-20
-40
-60
-80
-100
+6%
-4.6%
+14%
a)
PR
TMI
COM
Algorithm

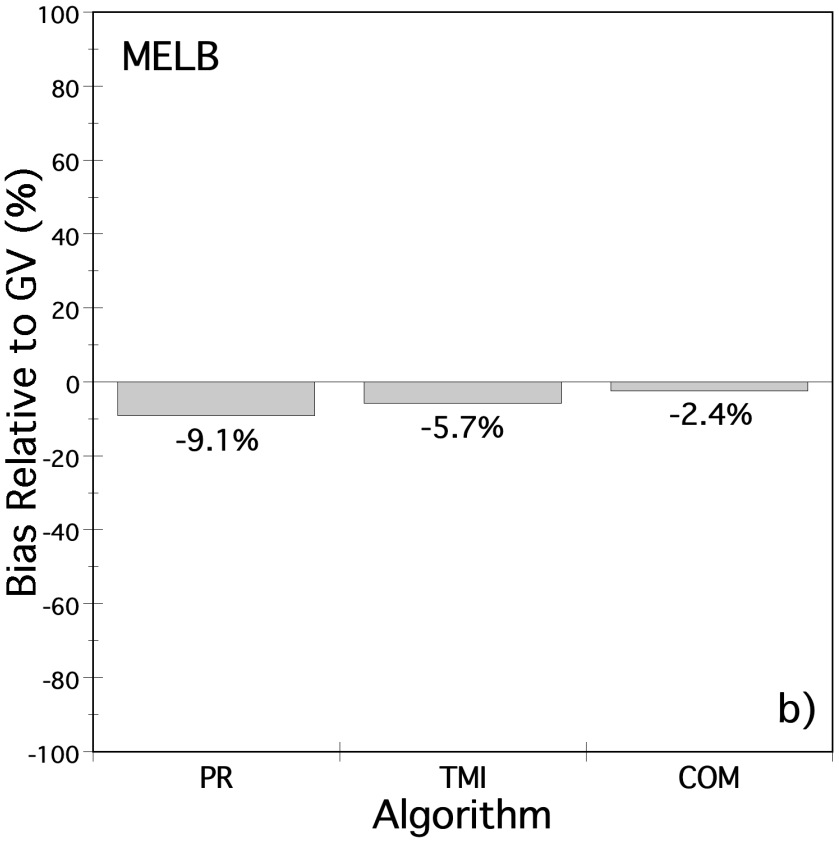
MELB
Bias Relative to GV (%)
100
80
60
40
20
0
-20
-40
-60
-80
-100
-9.1%
-5.7%
-2.4%
b)
PR
TMI
COM
Algorithm

Fig. 18: Bias of TRMM satellite estimates relative to GV for the period Jan. 2001 through Apr. 2002 for a) KWAJ and b) MELB. These biases are calculated by comparing the mean rain rate over 0.5° x 0.5° pixels in the GV domain. Only pixels that were considered as "ocean" by the TRMM satellite algorithms are shown. The bias is defined as the difference between the GV and satellite and GV mean for the period, normalized to the GV mean and is expressed in Eq. 1 in the text.

Table 1: Characteristics of the Kwajalein (KPOL) radar located on Kwajalein Island at the southern tip of Kwajalein Atoll in the Republic of the Marshall Islands.

***Kwajalein KPOL Radar Characteristics***

| | |
|---|---|
| *Frequency Range:* | 2800 MHz |
| *Peak Power:* | 700 kW @ 58.5 dB |
| *Normal Power:* | 500 kW |
| *Pulse width:* | 1.67 x $10^{-6}$ s |
| *PRF Intensity:* | 264-1536 Hz |
| *Radar Range (maximum)* | 270 nm |
| *Velocity:* | 150 km (81 nm) |
| *Antenna Gain:* | 43.8 dB |
| *Antenna Diameter:* | 8.2m (27 ft) |
| *Antenna Beamwidth:* | 0.95° |
| *Height to Center of Antenna:* | 20.7 m (68 ft) |
| *Input Power:* | 110/220 V single phase @ 7.5-10.0 kW |

Table 2: Task configuration for KPOL radar. Columns are: task name, radar polarization, azimuth sweep rate in deg s-1, elevation angles in degrees, pulse repetition frequency (PRF), and run time in minutes and seconds.

| *Tasks* | *Polar.* | *Rate* | *Elev. Angles* | *PRF* | *Time* |
|---|---|---|---|---|---|
| Surv_TRMM | Hor. | 8 | 1.0 | 396 | 00:53 |
| GVVOL_A | Dual | 15 | 0.4, 2.3, 4.2, 6.1, 8.0, 9.9, 11.8, 14.0, 16.6, 19.6, 23.2, 27.6 | 960 | 05:25 |
| GVVOL_B | Dual | 15 | 0.4, 1.4, 3.3, 5.2, 7.1, 9.0, 10.9, 12,9, 15.2, 18.0, 21.3, 25.3 | 960 | 05:25 |

Table 3: Description of the available networks, number of locations, gauge types and tipping-bucket rain increment for the four TRMM GV sites.

| GV SITE | Gauge Network | No. Gauge Sites | Rain Increment (mm) |
|---|---|---|---|
| Kwajalein | Kwajalein | 7 | 0.254 |
| Melbourne | St. Johns WMD | 27 | 0.254 |
| | NASA Kennedy Space Center | 33 | 0.254 |
| | South Florida WMD | 129 | 0.254 |
| | Triple-N Ranch | 20 | 0.254 |
| Houston | Harris County | 165 | 1.000 |
| Darwin | Darwin C-Scale | 33 | 0.200 |

Table 4: Description of the primary TRMM Standard Products (TSP) produced for Ground Validation.

| *Product* | *Fields* | *Description* |
|---|---|---|
| 1B-51 | DZ, VR, ZDR | Original coordinates and fields. Maximum range 230 km. |
| 1C-51 | CZ, DZ, VR | Original coordinates. CZ contains quality-controlled DZ field, Maximum range 200 km. HDF format. |
| 2A-52 | Echo coverage | Percentage echo coverage with satellite coincidence. ASCII format. |
| 2A-53 | R | Cartesian grid (2 km x 2 km, 151 x 151 pixels). Instantaneous rain intensity (mm hr-1). Maximum range 150 km. HDF format. |
| 2A-54 | Rain Type | Cartesian grid (2 km x 2 km, 151 x 151 pixels). Rain type (stratiform or convective). Maximum range 150 km. HDF format. From Steiner et al. (1995) |
| 2A-55 | CZ | 3-dimensional Cartesian Grid (2 km x 2 km horizontal, 1.5 km vertical; 151 x 151 x 13 pixels). Quality-controlled reflectivity. Maximum range 150 km. Maximum height 19.5 km. HDF format. |
| 2A-56 | R | 1-minute average gauge rain rates. One file per month, per gauge. ASCII format. |
| 3A-53 | R | Cartesian grid (2 km x 2 km). Five-day integrated rainfall. Maximum range 150 km. HDF format. |

| | | |
|---|---|---|
| 3A-54 | R | Cartesian grid (2 km x 2 km). Monthly-integrated rainfall. Maximum range 150 km. HDF format. |
| 3A-55 | R | 3-dimensional monthly structure with vertical profiles. HDF format. |

Table 5: Results of Validation comparisons between gauge-measured monthly rainfall and those of WPMM radar estimates. There are three types of validation: 1) IND: fully independent, in which gauges that are used for validation are not used for determination of the WPMM probabilities; 2) DEP: dependent, in which gauges that are used for determination of the calibration are also used for validation; and, 3) QUA: quasi-independent, in which a subset of the total number of gauges are excluded in the determination of the WPMM probabilities, but then are used for validation (see text for further details). Also shown are the periods over which the validations are made, the mean rainfall of the gauges and radar estimates, as well as the bias, relative to the gauge mean, expressed in percent, and the Mean Absolute Difference (MAD), defined as the mean absolute difference between the gauge and radar rain totals.

| Site | Val. Type | Period | Gauge Mean | Radar Mean | R/G | Bias (%) | MAD |
|---|---|---|---|---|---|---|---|
| MELB | DEP | 1998/08 | 180.47 | 179.10 | 0.99 | +1.0 | 0.16 |
| MELB | IND | 1998/08 | 135.08 | 145.23 | 1.08 | -7.5 | 0.09 |
| MELB | DEP | 1998/09 | 111.55 | 112.50 | 1.01 | -1.0 | 0.14 |
| MELB | QUA | 1998/09 | 190.01 | 177.63 | 0.93 | +6.5 | 0.12 |
| KWAJ | IND | 1997-2001 | 180.92 | 166.92 | 0.92 | +7.7 | 0.18 |

Table 6: Quasi-Independent Monthly Validation for Melbourne, Florida. Shown are the month and year, radar to gauge ratio, mean absolute deviation and the number of gauges that were used to derive the statistics.

| *Mon/Year* | *R/G Bias* | *MAD* | *Ng* |
|---|---|---|---|
| 11/1998 | 0.94 | 0.08 | 6 |
| 05/1999 | 1.02 | 0.19 | 9 |
| 06/1999 | 0.95 | 0.17 | 10 |
| 08/1999 | 1.00 | 0.16 | 9 |
| 09/1999 | 1.10 | 0.21 | 9 |
| 10/1999 | 1.08 | 0.10 | 9 |
| 07/2000 | 0.94 | 0.25 | 10 |
| 09/2000 | 0.92 | 0.28 | 10 |
| 06/2001 | 1.12 | 0.20 | 10 |
| 07/2001 | 1.07 | 0.21 | 10 |
| 08/2001 | 0.97 | 0.14 | 10 |
| 09/2001 | 0.96 | 0.10 | 10 |
| 06/2002 | 1.05 | 0.11 | 9 |
| 07/2002 | 0.90 | 0.23 | 11 |
| 08/2002 | 0.95 | 0.20 | 10 |
| 12/2002 | 1.04 | 0.09 | 7 |